

# LEARNING SPARSE ANALYTIC FILTERS FOR PIANO TRANSCRIPTION

Frank Cwitkowitz, Mojtaba Heydari, Zhiyao Duan

University of Rochester, Rochester, NY, USA

Department of Electrical and Computer Engineering

{fcwitkow,mheydari}@ur.rochester.edu zhiyao.duan@rochester.edu

## ABSTRACT

In recent years, filterbank learning has become an increasingly popular strategy for various audio-related machine learning tasks. This is partly due to its ability to discover task-specific audio characteristics which can be leveraged in downstream processing. It is also a natural extension of the nearly ubiquitous deep learning methods employed to tackle a diverse array of audio applications. In this work, several variations of a frontend filterbank learning module are investigated for piano transcription, a challenging low-level music information retrieval task. We build upon a standard piano transcription model, modifying only the feature extraction stage. The filterbank module is designed such that its complex filters are unconstrained 1D convolutional kernels with long receptive fields. Additional variations employ the Hilbert transform to render the filters intrinsically analytic and apply variational dropout to promote filterbank sparsity. Transcription results are compared across all experiments, and we offer visualization and analysis of the filterbanks.

## 1. INTRODUCTION

Automatic music transcription (AMT) is an essential capability for intelligent systems which analyze music [1]. The task is part of the broader music information retrieval (MIR) class of machine learning problems. AMT seeks to retrieve all of the information necessary to develop a score which accurately represents the music. However, given this complexity, the problem is typically reduced to the aim of estimating all notes, where a note is characterized by its pitch, time of onset, and duration [1]. Multi-instrument AMT is challenging, leading many to develop algorithms targeted for successful single-instrument AMT as an initial goal. In particular, piano transcription has been an active research task in AMT, given the wide availability of note annotations [2], and the consistency of piano timbre compared to multi-instrument ensembles [3].

Most machine learning methods involving AMT, and MIR in general, begin with a feature extraction stage which calculates a 2D time-frequency representation (TFR) for a piece of audio. Common choices for this step include the Mel-spectrogram or the constant-Q transform (CQT). In AMT algorithms, the features need to contain at least enough information to detect and track notes. While standard TFRs are viable for this purpose, they may not be optimal. In particular, most frequency analysis methods do

not explicitly model note characteristics. They also require careful design choices like filter shapes and other hyperparameters. Furthermore, there is fundamentally no information gained in moving to the frequency-domain.

In this work, we focus on filterbank learning for piano transcription, extending the preliminary work of [4]. Filterbank learning is a way to circumvent the use of hand-crafted features by replacing or augmenting the TFR calculation with the response from a bank of learnable filters. As the learnable filters are tuned jointly with a backend model for the task at hand, ideally they can model task- and domain-specific characteristics of the input signal.

Although filterbank learning is widely applicable to various audio processing problems, we target piano transcription because it is a complex task which, intuitively, may benefit from modeling notes in the time-domain. The filterbank learning paradigm provides an opportunity to model some of the more obscure properties of musical notes, such as onset or offset behavior, harmonic structure, inharmonicity, or more generally timbre. Piano transcription is also a task with plenty of annotated data and consistency, two characteristics which can simplify the problem.

We adopt the Onsets & Frames piano transcription model [2,5] and replace the feature extraction stage with a learnable filterbank module. We utilize a 1D convolutional structure for the filterbank, and experiment with several initialization strategies, model variations and regularization techniques. The filters represented in the module are complex, and can be employed with a standard hop size or stride. We compare the piano transcription results of each experiment, and provide an analysis of the learned filterbanks, visualizing and sonifying the filters. We show that in general, the filters converge to sparse, unique shapes, which we speculate to be modeling various note characteristics. Despite these interesting findings, the learned filterbanks still do not yet outperform fixed TFRs.

## 2. RELATED WORK

Filterbank learning has gained traction in recent years as a means to perform audio-related machine learning tasks in an end-to-end fashion. Some of the first filterbank learning attempts emerged to tackle problems within the speech community [6, 7], replacing the more widely used Mel-Frequency Cepstral Coefficients. This has led to powerful models for tasks such as speech separation [8, 9].

Filterbank learning has also been applied as a frontend

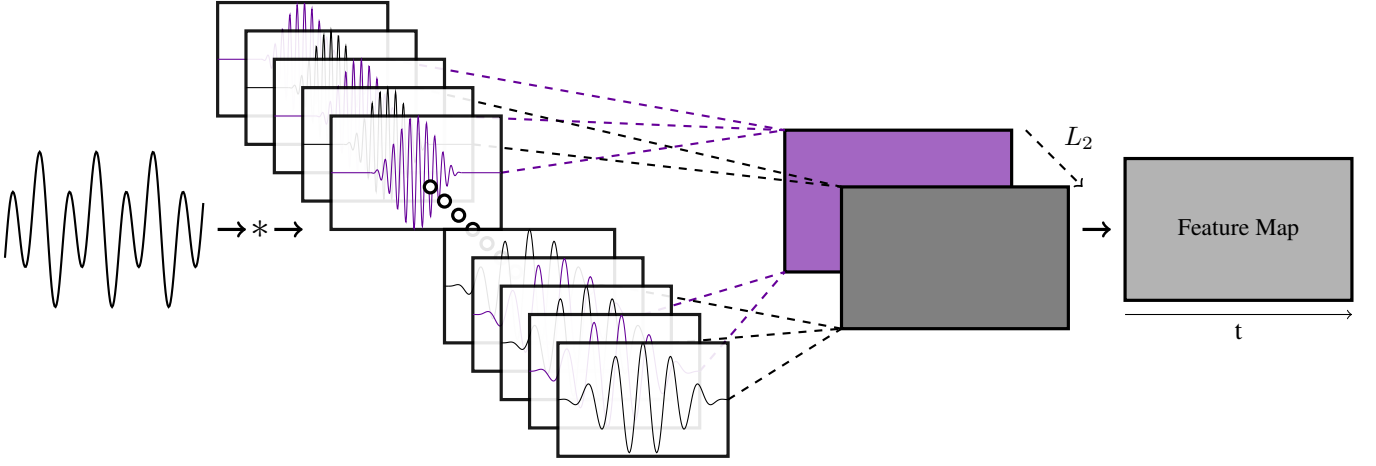


**Figure 1.** Complex filterbank learning module. The real (black) and imaginary (purple) part of each filter are learned independently. The real and imaginary responses are combined channel-wise using  $L_2$  pooling to obtain a feature map.

for music data. However, this has mainly been for high-level tasks such as music auto-tagging [10–12] or various classification problems [13, 14]. In contrast, filterbank learning for lower-level tasks, such as AMT, has received little attention. Music data has rich characteristics, patterns, and relationships at many layers of abstraction, including the note-level, the instrument-level, etc. As such, filterbank learning carries significant potential for discovering, capturing, and leveraging task-specific information.

Many filterbank learning approaches learn strictly real-valued filters, and attain shift-invariance by pooling the response at small hops across time [6]. These filterbanks are analogous to standard 1D convolutional blocks in deep networks. In contrast, the filters used in fixed TFR calculations, e.g., CQT, are typically complex and analytic, which means that they implicitly encode phase. As such, they are stable with relatively large hop sizes, and there is no need to apply further temporal pooling on their responses.

Some filterbank learning approaches have extended the 1D convolutional approach to implement complex filters with grouped real-valued filters representing the real and imaginary part of the complex filter [15–17]. While the filters in these examples are complex, if their analytic property is not preserved, they will have an asymmetric frequency response about 0 Hz and no longer exhibit shift-invariance in the magnitude response. Moreover, the 1D convolutional layer approach sometimes suffers from too little constraints, leading to noisy filters with no clear or localized frequency response. One way to address this is to add soft constraints, e.g., initializing the filterbank with the weights approximating a standard transform [6, 18].

Recently, there has been a trend to further constrain the filterbank learning paradigm [19, 20], by learning a small number of parameters which define fixed-shape filters. While these approaches may exhibit more stability, they can only really model simple bandpass filters and thus, lower the potential for discovering meaningful patterns in data at the signal level. Other approaches learn frequency-domain filters on top of spectrograms [21, 22], initializing them with harmonic relationships. We wish to

discover these relationships naturally, rather than imposing them as a constraint.

Many approaches to piano transcription have attempted to realize a framework which could learn task-specific note characteristics. Non-Negative Matrix Factorization (NMF) has been proposed as a viable framework for learning properties such as the harmonic relationships, temporal evolution, attack, and decay of piano notes from a TFR [23, 24]. Convolutional sparse coding is a similar approach which operates in the time-domain, and was proposed as a way to estimate the activation of pre-trained note impulse responses [3, 25].

More recently, deep neural networks (DNNs) have demonstrated success in learning to estimate discrete pitch activity from TFRs [2, 5, 26, 27]. Some approaches have attempted to design DNNs such that they naturally leverage information about note characteristics [28, 29]. Since they are very powerful and efficient at learning features for many tasks, we hypothesize that DNNs can be utilized to learn better feature maps for acoustic models. Furthermore, we believe this type of frontend will naturally model note characteristics for piano transcription.

### 3. METHOD

The complex filterbank learning module is implemented within a 1D convolutional layer. It accepts a 1D signal as input and produces a real and imaginary feature map, which are combined using  $L_2$  pooling, a simple mechanism for taking the magnitude. The output of the module is subsequently converted to log-amplitude and fed into a batch normalization layer. The filterbank is formulated such that an inner product is taken between a time-domain signal  $x$  and  $n_{bins}$  filters, indexed by  $\mu$ , of respective lengths  $l_\mu$  with weights  $\theta_\mu$  at discrete hops  $k$  spaced  $l_h$  samples apart:

$$X[k, \mu] = \sum_{n=0}^{l_\mu-1} x[kl_h + n]\theta_\mu[n]. \quad (1)$$

Note that this operation is equivalent to convolution, or more precisely correlation, using a stride of  $l_h$ . The most straightforward way to represent complex filters in this type of framework is to allocate two adjacent filters for the real and imaginary weights, and to combine their respective responses channel-wise using  $L_2$  pooling [15]:

$$X[k, \mu] = \sqrt{(x * \mathcal{R}(\theta_\mu))^2 + (x * \mathcal{I}(\theta_\mu))^2}. \quad (2)$$

Note that with this representation, there are actually  $2 \times n_{bins}$  filters to learn, and they are only implicitly associated via the subsequent pooling mechanism. Figure 1 illustrates this filterbank architecture. While this approach can model complex filters, the filters are rarely analytic, unless they are initialized as analytic filters. This means that they may have nonzero responses to negative frequencies and may not be shift-invariant with respect to time.

Another way to model complex filters is to learn only the real part and to infer the imaginary part such that the complex filter is analytic. This can be done using the Hilbert Transform [30], which computes the imaginary counterpart to a real signal, such that the resulting complex signal is analytic. This can be expressed as

$$X[k, \mu] = \sqrt{(x * \mathcal{R}(\theta_\mu))^2 + (x * H(\mathcal{R}(\theta_\mu)))^2}, \quad (3)$$

where  $H(\cdot)$  denotes the Hilbert transform. This variation learns more intuitive, shift-invariant filters with frequency responses containing only energy in the positive frequency range. It is important to note that the filters represented with this variation may only be approximately analytic, due to the limitations of discrete processing.

### 3.1 Initialization Strategy

Within the framework presented above, the weights  $\theta_\mu$  are initialized randomly by default. Without inserting any prior knowledge into the filterbank, it must learn to generate feature maps from scratch. This strategy has the potential to discover new filter shapes and characteristics that are not present in standard TFRs.

Alternatively, it is possible to insert weights into the filterbank such that it implements a time-domain variable-Q transform (VQT) if left untrained. The complex variable-Q response for filter  $\mu$  can be computed in the time-domain by making the weights  $\theta_\mu$  complex basis functions with center frequency  $f_\mu$ , sampling rate  $f_s$ , and smoothly varied Q-factor  $Q_\mu$ :

$$\theta_{\mu,n} = w_{\mu,n} e^{-j \frac{2\pi f_\mu n}{f_s}}, \quad n = 0, \dots, l_\mu. \quad (4)$$

The filter length  $l_\mu = \lceil Q_\mu \frac{f_s}{f_\mu} \rceil$  is set such that the desired Q-factor, whether constant or smoothly varied, is maintained across all filters. The windowing function  $w$  is chosen as a Hanning window and matches the filter length  $l_\mu$  for each filter. We avoid normalizing the response of each basis by filter length  $l_\mu$  so that the weights of each filter are all comparable and responsive to a single learning rate. The center frequency of each filter in the VQT

initialization is defined by selecting an  $f_{min}$ , and applying

$$f_\mu = f_{min} \times 2^{\frac{\mu}{n_{bpo}}}, \quad (5)$$

where  $n_{bpo}$  is the number of bins or per octave.

The bandwidth of each respective filter is determined by  $B_\mu = f_{\mu+1} - f_\mu + \gamma$ . In a CQT, the ratio between the center frequency  $f_\mu$  and the bandwidth  $B_\mu$ , or the Q-factor, is constant, meaning that  $\gamma = 0$ . However, for large  $n_{bpo}$ , this can lead to filters with extremely tight bands, which require long impulse responses. Modestly utilizing the constant bandwidth offset  $\gamma$  relaxes the constancy constraint in the lower frequency range and provides direct control over the size of the filter receptive fields, which must all be zero-padded to the largest filter in order to be stored in a 1D convolutional layer. We also use the VQT parameters to determine the receptive field size for random initialization.

Initializing the filterbank with the VQT weights provides a solid base with which to improve upon, and could even be thought of as pre-training the filterbank. Although there are multiple transforms one could utilize in acquiring the initial weights, the VQT is chosen because it is intuitively a better starting point for modeling note characteristics. Every  $\frac{n_{bpo}}{12}$  filter is already locked onto a pitch in the Western music scale. Since we are primarily concerned with relationships between pitch and temporal characteristics for the AMT problem, we believe this is an appropriate initialization strategy.

One additional initialization strategy is the harmonic comb, where a set of harmonics  $\mathcal{H}$  is defined, and separate filters with center frequency  $f = h \times f_\mu$  are constructed for each  $h \in \mathcal{H}$ . All filters associated with a given  $\mu$  are summed and collapsed into a single set of weights for insertion into the 1D convolutional layer. In this way, each filter responds directly to the harmonics of its corresponding pitch, and characteristics such as inharmonicity or relative harmonic strength (timbre) can be fine-tuned.

### 3.2 Variational Dropout

Variational dropout [31] is a regularization technique which allows for the learning of sparse frontend filters with long receptive fields. It is similar to Gaussian dropout, except the dropout rate, or variance, corresponding to each weight is learned. During training we treat the weights as random variables, with their true values  $\theta$  being the mean, and an additional set of learned parameters  $\sigma^2$  being their variance. By learning the variance of each weight, variational dropout induces sparsity, as it pushes less important weights to have higher variance, and more important weights to have lower variance. This leads to more sparse and interpretable filters, and can deal with very long receptive fields effectively. The stochasticity can also stimulate the filterbank to take interesting and unexpected shapes as it is being trained. During each forward pass, noise is sampled from the variance of the filterbank response and added to the mean response:

$$X[k, \mu] \sim \mathcal{N}(x * \theta_\mu, x^2 * \sigma_\mu^2). \quad (6)$$

The parameters  $\sigma_\mu^2$  are jointly trained with the filterbank parameters  $\theta_\mu$ , and their gradient is calculated using a very close approximation to the KL-divergence [31]. In practice, we iterate upon  $\log \sigma^2$  for improved stability. It should be noted that we only add noise to the real part of the feature map when using the Hilbert filterbank variant.

## 4. EXPERIMENTS

### 4.1 Model

The filterbank learning module is used as a replacement for the frontend of the Onsets & Frames model [2, 5] and jointly trained for the task of piano transcription. The Onsets & Frames model takes as input a Mel spectrogram and produces a frame-wise salience estimate for note pitches, independently. Note predictions are generated using the simple post-processing steps proposed in the original paper, but we do not use the note predictions to refine the frame-wise salience, nor do we attempt to perform the additional velocity estimation step. Our experimental setup is the same as the original Onsets & Frames paper [5] with the subsequent improvements proposed in a follow-up paper [2]. We implemented the model from scratch<sup>1</sup> and verified that the results were consistent with what was previously reported (see Section 4.4). We utilize the same hyperparameters, running each experiment for 2000 iterations, where each music piece is accessed only once per iteration to sample a sequence of frames for a batch.

### 4.2 Datasets

The MAESTRO dataset [2] is used for training, validation, and testing. Specifically, we use version 3 ( $V_3$ ) of the dataset for all but one experiment, which is run on version 1 ( $V_1$ ). We follow the suggested partitioning for both versions. We also evaluate on the acoustic partitions (ENSTDkAm/ENSTDkCl) of the MAPS dataset [32], to inspect the generalization potential of our method. For all experiments, we downsample the audio to  $f_s = 16,000$  Hz, and use a hop length of  $L_h = 512$  samples.

### 4.3 Metrics

We evaluate experiments using the same transcription metrics as in [5], which include frame-wise, note-wise, and note-wise with offset scores. Each of these metrics is calculated in terms of precision, recall, and f1-score, using `mir_eval` [33]. For frame-wise evaluation, detected pitches are compared to the ground-truth at the frame level. For note-wise evaluation, note estimates for an entire piece are compared to the ground-truth. A note is considered correct if its pitch is within half a semitone of the true value, and if its onset is within 50 ms of the true value. The note-wise with offset metric additionally compares the estimated offset to the true value, a correct estimate being within 50 ms or 20% of the ground truth duration, whichever is larger.

<sup>1</sup> All code is available at <https://github.com/cwitkowitz/sparse-analytic-filters>.

### 4.4 Results

We conduct several baseline experiments to verify our implementation of Onsets & Frames, and to assess the strength of various features. For Mel spectrogram, we use  $n_{bins} = 229$  and HTK frequency spacing, as in [2]. For CQT and VQT we choose  $f_{min} \approx 32.7$  Hz,  $n_{bins} = 252$  and  $n_{bpo} = 36$ , or 3 bins per semitone. For the VQT experiment, we calculate  $\gamma = \frac{24.7}{0.108 * Q}$ , such that all filters have a bandwidth proportional to the ERB scale by a constant factor [34]. We also experiment with an untrained filterbank initialized using the harmonic comb strategy ( $\mathcal{H} = \{1, \dots, 10\}$ ). The results for these baseline experiments are provided at the top of Table 1.

We observe that Mel spectrogram performs best in every metric besides note-onsets for MAPS, where the untrained comb filterbank only slightly outperforms it. Interestingly, the comb filterbank is inferior in all other metrics.

Next we conduct several filterbank learning experiments where the feature map output of the filterbank is fed to the model instead of a TFR. The same VQT parameters used in the baseline experiments are used to initialize the filterbanks. We vary the filterbank variant, initialization, and regularization method across all experiments. For Gaussian and variational dropout, we initialize all  $\log \sigma_{\mu,n}^2 = -10$ , and for Bernoulli dropout we use a dropout rate of 10%. For variational dropout, the KL-divergence term is scaled by a factor of 0.01, such that the implicit sparsity objective does not completely dominate the training procedure. The results for these filterbank experiments are provided at the bottom of Table 1.

The Hilbert transform-based architecture slightly improves upon the classic framework. The filterbanks initialized with VQT weights slightly outperform the randomly initialized filterbanks. The variational dropout regularization method performs the best, though still underneath the experiments that had no regularization. For the variational dropout experiments, the harmonic comb initialization outperforms the VQT initialization for note metrics but not frame metrics. None of the learned filterbanks outperform the fixed calculations, however they nonetheless demonstrate reasonable performance, even when initialized randomly. The learned filterbanks, however, do not seem to generalize very well to the MAPS dataset.

## 5. DISCUSSION

### 5.1 General

The reduced performance of the filterbank learning models can potentially be attributed to too little training or inadequate tuning of hyperparameters. We also speculate that the consistency of piano data, coupled with large model complexity, may have led to overfitting, as evidenced by the lack of generalization to the MAPS dataset. Furthermore, state-of-the-art methods which do not use filterbank learning, already perform piano transcription reasonably well. As such, it may be that a similar filterbank learning approach would show much more promise in areas with



Experiment	MAESTRO			MAPS		
	Frame $F_1$	Note-On $F_1$	Note-Off $F_1$	Frame $F_1$	Note-On $F_1$	Note-Off $F_1$
<i>mel</i>	91.80*	95.95*	83.44*	81.40*	81.42*	59.15*
<i>mel</i>	<b>90.91</b>	<b>95.82</b>	<b>83.14</b>	<b>81.26</b>	83.86	<b>59.07</b>
<i>cqt</i>	90.79	95.29	82.30	77.46	82.35	52.18
<i>vqt</i>	90.18	94.74	80.51	80.26	83.42	55.34
<i>fixed comb</i>	86.91	91.76	74.24	78.77	<b>83.89</b>	54.71
<i>cl+rnd</i>	86.62	91.11	73.23	69.29	79.05	41.79
<i>cl+vqt</i>	87.48	92.49	74.99	75.41	80.48	51.43
<i>hb+rnd</i>	86.74	91.63	74.97	70.87	79.74	44.35
<i>hb+vqt</i>	<b>88.06</b>	<b>93.01</b>	<b>76.87</b>	74.00	80.92	49.61
<i>hb+rnd+brn</i>	84.87	90.05	70.12	74.73	78.89	50.28
<i>hb+rnd+gau</i>	86.31	90.95	73.24	72.33	79.10	47.20
<i>hb+rnd+var</i>	86.52	91.58	74.43	71.87	79.87	45.94
<i>hb+vqt+var</i>	86.86	91.39	73.65	<b>75.75</b>	80.11	<b>51.69</b>
<i>hb+comb+var</i>	86.76	91.80	74.12	75.32	<b>81.37</b>	51.29

**Table 1.** Evaluation results for all baseline and filterbank experiments (separated by break). Filterbank learning experiment names are formatted in terms of variant (classic (*cl*) / Hilbert (*hb*)) + initialization (random (*rnd*) / *vqt* / *comb*) + dropout (none / Bernoulli (*brn*) / Gaussian (*gau*) / variational (*var*)). Results obtained using MAESTRO  $V_1$  are indicated by \*.

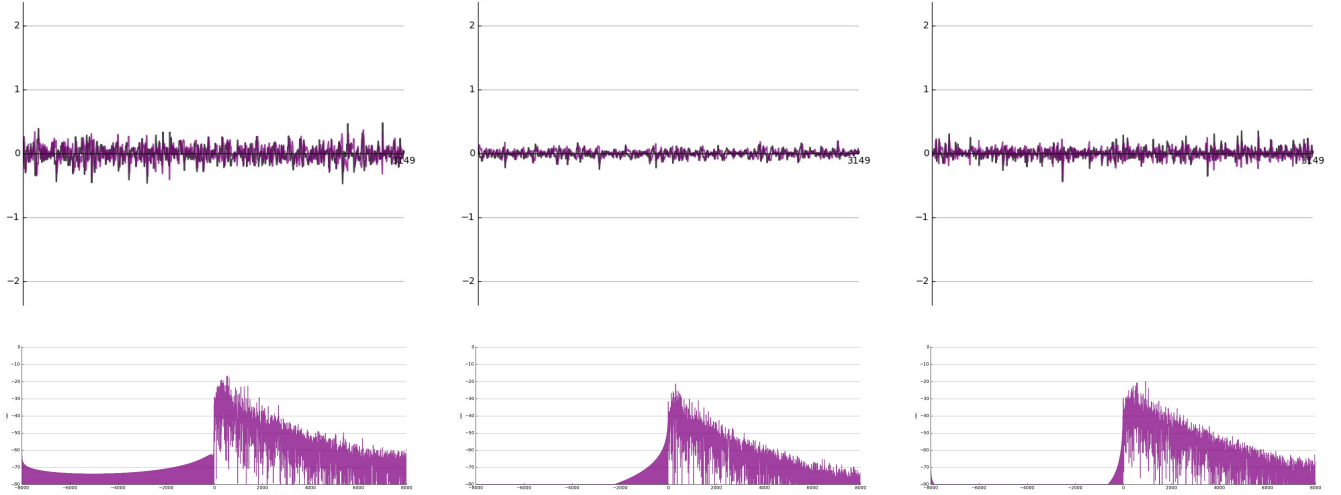


**Figure 2.** Examples of filters from the *hb+rnd+var* experiment which exhibit a higher degree of sparsity.

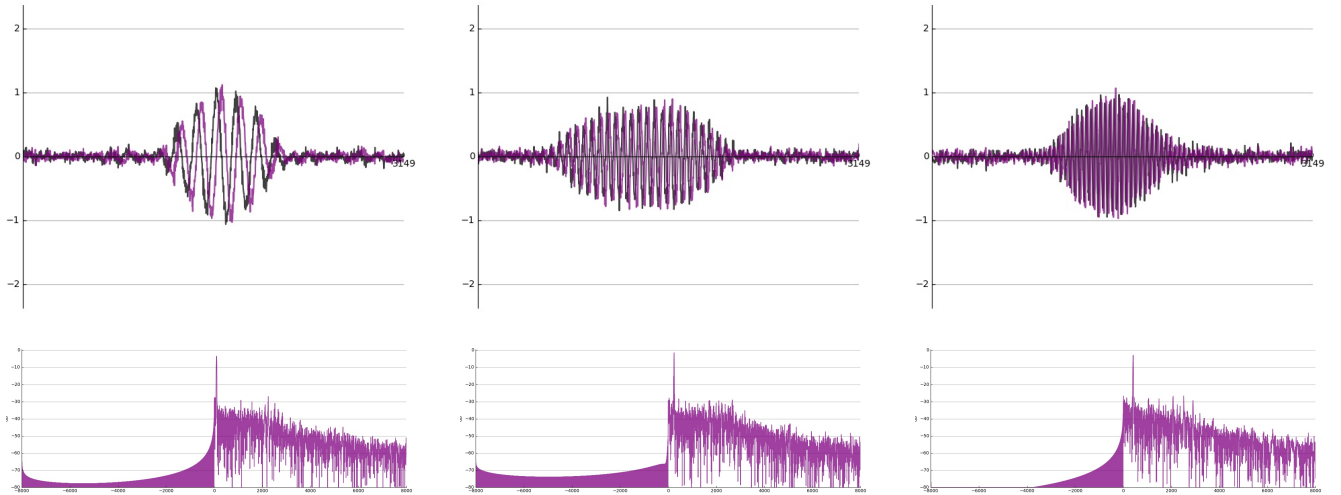


**Figure 3.** Examples of filters from the *hb+rnd+var* experiment which are well-localized within the receptive field and exhibit coherent shapes in both the time- and frequency-domain.

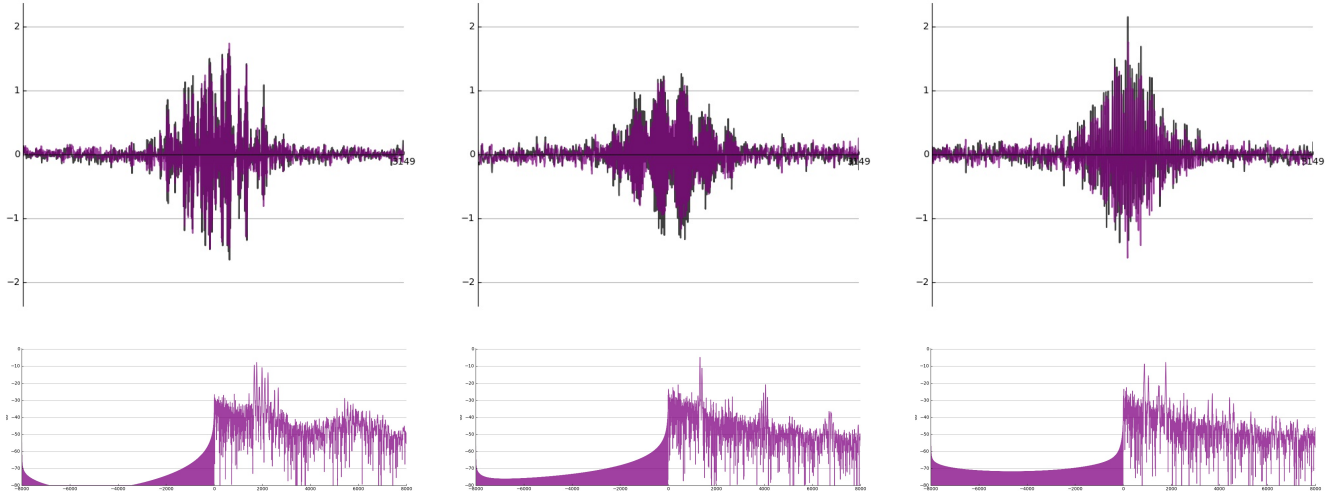


**Figure 4.** Examples of filters from the *hb+rnd+var* experiment which support multiple frequencies.

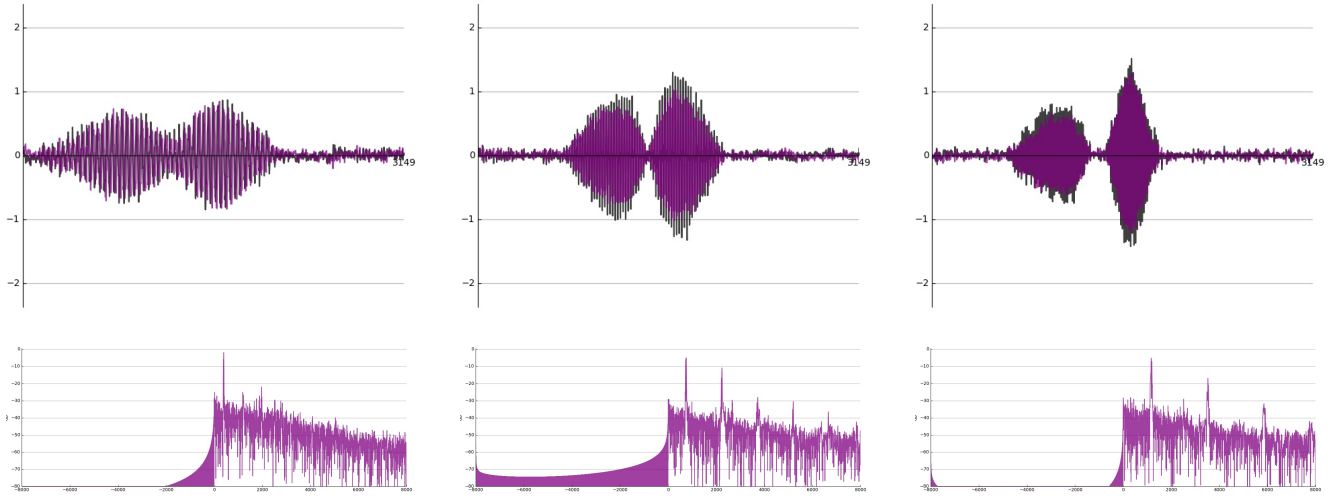


**Figure 5.** Examples of filters from the *hb+rnd+var* experiment which appear to model the attack and decay of notes.

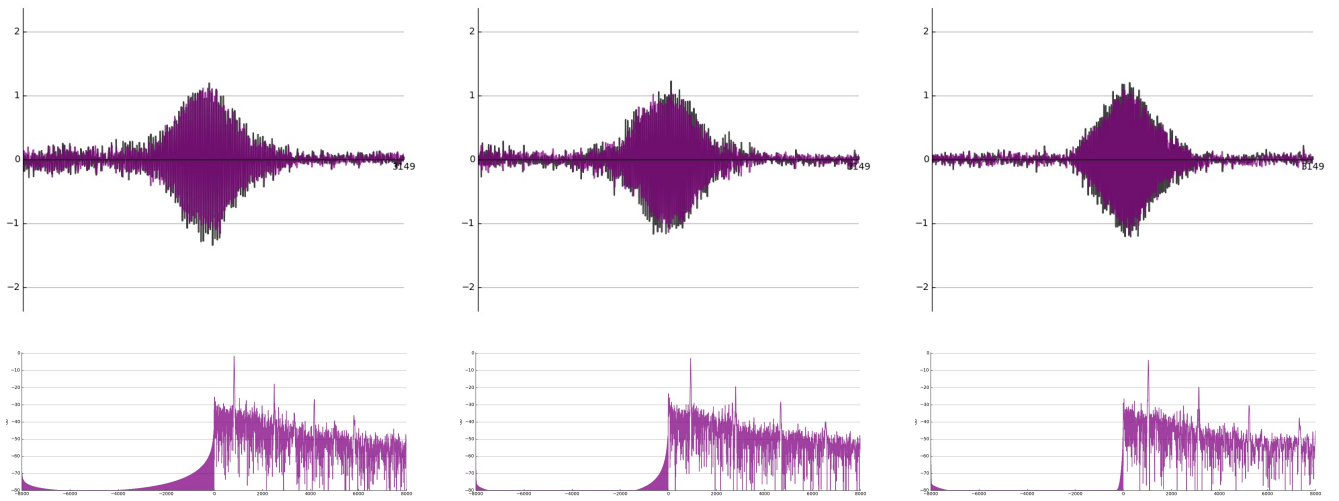


**Figure 6.** Examples of filters from the *hb+rnd+var* experiment which exhibit a clear harmonic structure.

less data and less consistency, such as drum or guitar transcription.

## 5.2 Visualization

We provide a visualization for a few examples from the filterbank learning experiment corresponding to the Hilbert variant with random initialization and variation dropout (*hb+rnd+var*), which we consider to have produced the most interesting filters. Due to lack of space, we provide similar materials for the other filterbank learning experiments in the Appendix. Several filters belonging to different categories of learned filters for the *hb+rnd+var* experiment are presented in Figures 2-6. In each figure, the time-domain visualization for three filters is displayed in the top row, with the corresponding frequency-domain visualization for each respective filter in the bottom row. The specific examples are chosen for no reason other than that they appear to belong to the same category of learned filter.

In general, the filters learned for the *hb+rnd+var* experiment tend to exhibit a high degree of sparsity, with many encompassing coherent shapes in both the time- and frequency-domain. Figure 2 and Figure 3 illustrate these properties, respectively. The non-zero filter weights tend to be well-localized within the receptive field, with weights closer to zero being closer to the edges and more prominent weights being closer to the center. The tendency of the filters to be sparse is highly desirable, as it encourages more modular filters and leads to more interpretable shapes in time and frequency. Indeed, it appears that the importance of a filter can be directly estimated from its amplitude, with less important or even unused filters consisting of mostly near-zero weights rather than random noise, as is the case with other filterbank learning variants and approaches (See Appendix). Furthermore, all of the Hilbert variant filters remain approximately analytic throughout the training process. We do not view the artifacts in the negative frequency range to be problematic, and believe they had a negligible effect on the outcome of experiments.

Some additional interesting qualities of the filters are observed, which are presumably related to the modeling of domain-specific characteristics for piano transcription. The spectrum of the filters in Figure 4 include multiple prominent fundamental frequencies in clusters, which suggests the filters may be modeling harmony or polyphonic piano sounds of some sort. The filters in Figure 5 appear to be modeling the attack and decay of a piano note with the same pitch. This judgement is made due to the fact that the spectrums of these filters show only one prominent fundamental frequency, while the impulse responses of the filters encapsulate two approximately symmetric nodes. Some of these filters, in addition to the filters in Figure 6, exhibit harmonic patterns in the frequency spectrum. In particular, odd harmonics tend to be emphasized in these filters. These observations suggest that the proposed filterbank learning approach is capable of capturing lower-level features which are relevant for music transcription, and that the approach is likely extensible to similar tasks where this type of information would be beneficial.

## 5.3 Sonification

In order to analyze the filters in the auditory domain, we time stretch them by 5x and convert the real part of the filters to audio. In general, the noisy near-zero filters sound like piano fluctuating through a monochromatic scale. Irrelevant or less important harmonic information was likely dumped into these filters during the training process. Distinct frequencies can be heard when listening to the filters with more coherent shapes. Filters with harmonic structure in the spectra tend to sound more musical and less sinusoidal than filters with no prominent harmonic frequencies. Filters with multiple prominent fundamental frequencies produce more complex sounds, but it is hard to infer their precise relevance or context. The filters with impulse responses encapsulating two nodes sound like a single pitch being ramped up and then ramped down. In some cases, adjacent filters sound like they are modeling the same frequency, suggesting there may be some important distinction or some complementary effect.

## 6. CONCLUSION

A filterbank learning module and various techniques were analyzed for the task of piano transcription, resulting in many interesting learned filters. It is not entirely clear why the filterbank learning module converged to the presented filters, but there are several reasons to suggest that the filters may be modeling note characteristics, such as attack and decay, harmonic structure and relative strength, or inharmonicity. As progress continues, it is important to leave the filterbank learning module as unconstrained as possible, so that unique and potentially better task-specific filters can be learned. It is also necessary to structure and regularize the learning process such that it can lead to sparse and intrinsically shift-invariant filters. Lastly, it is also helpful to inspect resulting filters in order to better understand the filterbank learning process, so that it may be improved. In this work, we showed that it is possible to learn sparse filters from scratch, and that they differ significantly from those of the fixed transforms. Although the learned filterbanks did not surpass the performance of the fixed transforms, our method shows promise in learning to model note characteristics in the time-domain.

## 7. ACKNOWLEDGMENTS

This work has been funded by the National Science Foundation grants IIS-1846184 and DGE-1922591. We would also like to thank Dr. Juan Cockburn and Dr. Andres Kwasinski for their guidance during the Master's Thesis [4] that set the stage for this work.

## 8. REFERENCES

- [1] E. Benetos, S. Dixon, Z. Duan, and S. Ewert, “Automatic music transcription: An overview,” *IEEE Signal Processing Magazine*, vol. 36, no. 1, pp. 20–30, 2019.
- [2] C. Hawthorne, A. Stasyuk, A. Roberts, I. Simon, C.-Z. A. Huang, S. Dieleman, E. Elsen, J. Engel, and D. Eck, “Enabling factorized piano music modeling and generation with the MAESTRO dataset,” in *Proceedings of the International Conference on Learning Representations (ICLR)*, 2019.
- [3] A. Cogliati, Z. Duan, and B. Wohlberg, “Piano music transcription with fast convolutional sparse coding,” in *Proceedings of the IEEE 25th International Workshop on Machine Learning for Signal Processing (MLSP)*, 2015.
- [4] F. Cwitkowitz, “End-to-end music transcription using fine-tuned variable-Q filterbanks,” Master’s thesis, Rochester Institute of Technology, 2019.
- [5] C. Hawthorne, E. Elsen, J. Song, A. Roberts, I. Simon, C. Raffel, J. Engel, S. Oore, and D. Eck, “Onsets and frames: Dual-objective piano transcription,” in *Proceedings of the 19th International Society for Music Information Retrieval Conference (ISMIR)*, 2018.
- [6] T. N. Sainath, R. J. Weiss, A. Senior, K. W. Wilson, and O. Vinyals, “Learning the speech front-end with raw waveform CLDNNs,” in *Proceedings of Interspeech*, 2015.
- [7] Y. Hoshen, R. J. Weiss, and K. W. Wilson, “Speech acoustic modeling from raw multichannel waveforms,” in *Proceedings of the IEEE International Conference on Acoustics, Speech and Signal Processing (ICASSP)*, 2015.
- [8] Y. Luo and N. Mesgarani, “TasNet: Time-domain audio separation network for real-time, single-channel speech separation,” in *Proceedings of the IEEE International Conference on Acoustics, Speech and Signal Processing (ICASSP)*, 2018.
- [9] —, “Conv-TasNet: Surpassing ideal time–frequency magnitude masking for speech separation,” *IEEE/ACM Transactions on Audio, Speech, and Language Processing (TASLP)*, vol. 27, no. 8, pp. 1256–1266, 2019.
- [10] S. Dieleman and B. Schrauwen, “End-to-end learning for music audio,” in *Proceedings of the IEEE International Conference on Acoustics, Speech and Signal Processing (ICASSP)*, 2014.
- [11] J. Pons, O. Nieto, M. Prockup, E. Schmidt, A. Ehmann, and X. Serra, “End-to-end learning for music audio tagging at scale,” in *Proceedings of the 19th International Society for Music Information Retrieval Conference (ISMIR)*, 2018.
- [12] T. Kim, J. Lee, and J. Nam, “Sample-level cnn architectures for music auto-tagging using raw waveforms,” in *Proceedings of the IEEE International Conference on Acoustics, Speech and Signal Processing (ICASSP)*, 2018.
- [13] J. Lee, J. Park, K. L. Kim, and J. Nam, “SampleCNN: End-to-end deep convolutional neural networks using very small filters for music classification,” *Applied Sciences*, vol. 8, no. 1, 2018.
- [14] J. Thickstun, Z. Harchaoui, and S. Kakade, “Learning features of music from scratch,” in *Proceedings of the International Conference on Learning Representations (ICLR)*, 2017.
- [15] N. Zeghidour, N. Usunier, I. Kokkinos, T. Schaiz, G. Synnaeve, and E. Dupoux, “Learning filterbanks from raw speech for phone recognition,” in *Proceedings of the IEEE International Conference on Acoustics, Speech and Signal Processing (ICASSP)*, 2018.
- [16] N. Zeghidour, N. Usunier, G. Synnaeve, R. Collobert, and E. Dupoux, “End-to-End Speech Recognition from the Raw Waveform,” in *Proceedings of Interspeech*, 2018.
- [17] S. Lattner, M. Dörfler, and A. Arzt, “Learning complex basis functions for invariant representations of audio,” in *Proceedings of the 20th International Society for Music Information Retrieval Conference (ISMIR)*, 2019.
- [18] K. W. Cheuk, H. Anderson, K. Agres, and D. Herremans, “nnAudio: An on-the-fly GPU audio to spectrogram conversion toolbox using 1D convolutional neural networks,” *IEEE Access*, vol. 8, pp. 161 981–162 003, 2020.
- [19] M. Ravanelli and Y. Bengio, “Speaker recognition from raw waveform with SincNet,” in *Proceedings of the IEEE Spoken Language Technology Workshop (SLT)*, 2018.
- [20] N. Zeghidour, O. Teboul, F. d. C. Quitry, and M. Tagliasacchi, “LEAF: A learnable frontend for audio classification,” in *Proceedings of the International Conference on Learning Representations (ICLR)*, 2021.
- [21] M. Won, S. Chun, O. Nieto, and X. Serra, “Data-driven harmonic filters for audio representation learning,” in *Proceedings of the IEEE International Conference on Acoustics, Speech and Signal Processing (ICASSP)*, 2020.
- [22] Z. Zhang, Y. Wang, C. Gan, J. Wu, J. B. Tenenbaum, A. Torralba, and W. T. Freeman, “Deep audio priors emerge from harmonic convolutional networks,” in *Proceedings of the International Conference on Learning Representations (ICLR)*, 2020.

- [23] E. Vincent, N. Bertin, and R. Badeau, “Adaptive harmonic spectral decomposition for multiple pitch estimation,” *IEEE Transactions on Audio, Speech, and Language Processing (TASLP)*, vol. 18, no. 3, pp. 528–537, 2010.
- [24] T. Cheng, M. Mauch, E. Benetos, S. Dixon *et al.*, “An attack/decay model for piano transcription,” in *Proceedings of the 17th International Society for Music Information Retrieval Conference (ISMIR)*, 2016.
- [25] A. Cogliati, Z. Duan, and B. Wohlberg, “Piano transcription with convolutional sparse lateral inhibition,” *IEEE Signal Processing Letters*, vol. 24, no. 4, pp. 392–396, 2017.
- [26] S. Sigtia, E. Benetos, and S. Dixon, “An end-to-end neural network for polyphonic piano music transcription,” *IEEE/ACM Transactions on Audio, Speech, and Language Processing (TASLP)*, vol. 24, no. 5, pp. 927–939, 2016.
- [27] R. Kelz, M. Dorfer, F. Korzeniowski, S. Böck, A. Arzt, and G. Widmer, “On the potential of simple framewise approaches to piano transcription,” in *Proceedings of the 17th International Society for Music Information Retrieval Conference (ISMIR)*, 2016.
- [28] R. Kelz, S. Böck, and G. Widmer, “Deep polyphonic ADSR piano note transcription,” in *Proceedings of the IEEE International Conference on Acoustics, Speech and Signal Processing (ICASSP)*, 2019.
- [29] T. Kwon, D. Jeong, and J. Nam, “Polyphonic piano transcription using autoregressive multi-state note model,” in *Proceedings of the 21st International Society for Music Information Retrieval Conference (ISMIR)*, 2020.
- [30] M. Pariente, S. Cornell, A. Deleforge, and E. Vincent, “Filterbank design for end-to-end speech separation,” in *Proceedings of the IEEE International Conference on Acoustics, Speech and Signal Processing (ICASSP)*, 2020.
- [31] D. Molchanov, A. Ashukha, and D. Vetrov, “Variational dropout sparsifies deep neural networks,” in *Proceedings of the 34th International Conference on Machine Learning (ICML)*, 2017.
- [32] V. Emiya, R. Badeau, and B. David, “Multipitch estimation of piano sounds using a new probabilistic spectral smoothness principle,” *IEEE Transactions on Audio, Speech, and Language Processing (TASLP)*, vol. 18, no. 6, pp. 1643–1654, 2010.
- [33] C. Raffel, B. McFee, E. J. Humphrey, J. Salamon, O. Nieto, D. Liang, D. P. Ellis, and C. C. Raffel, “mir\_eval: A transparent implementation of common MIR metrics,” in *Proceedings of the 15th International Society for Music Information Retrieval Conference (ISMIR)*, 2014.
- [34] C. Schörkhuber, A. Klapuri, N. Holighaus, and M. Dörfler, “A matlab toolbox for efficient perfect reconstruction time-frequency transforms with log-frequency resolution,” in *Audio Engineering Society (AES) 53rd Conference on Semantic Audio*, 2014.

## 9. APPENDIX

Here we provide some additional visualization for the filters learned during auxiliary experiments. The visualization is by no means exhaustive. However, the exemplified filters should be sufficient as representatives for each respective experiment.

### 9.1 Hilbert + Random + Variational (hb+rnd+var)

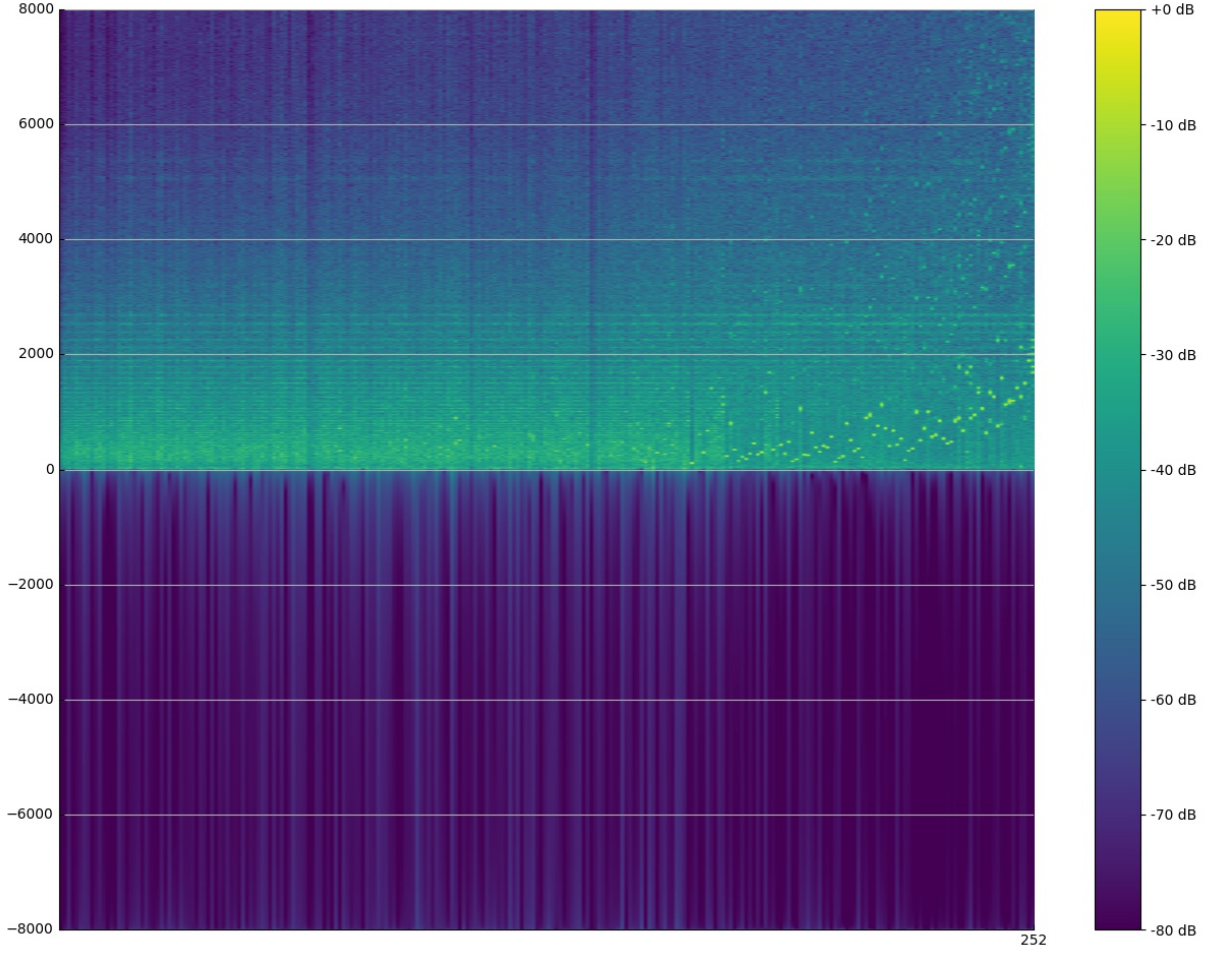


**Figure 7.** Frequency response of the entire filterbank for the *hb+rnd+var* (main) experiment, ordered by spectral centroid.



## 9.2 Classic + Random (cl+rnd)

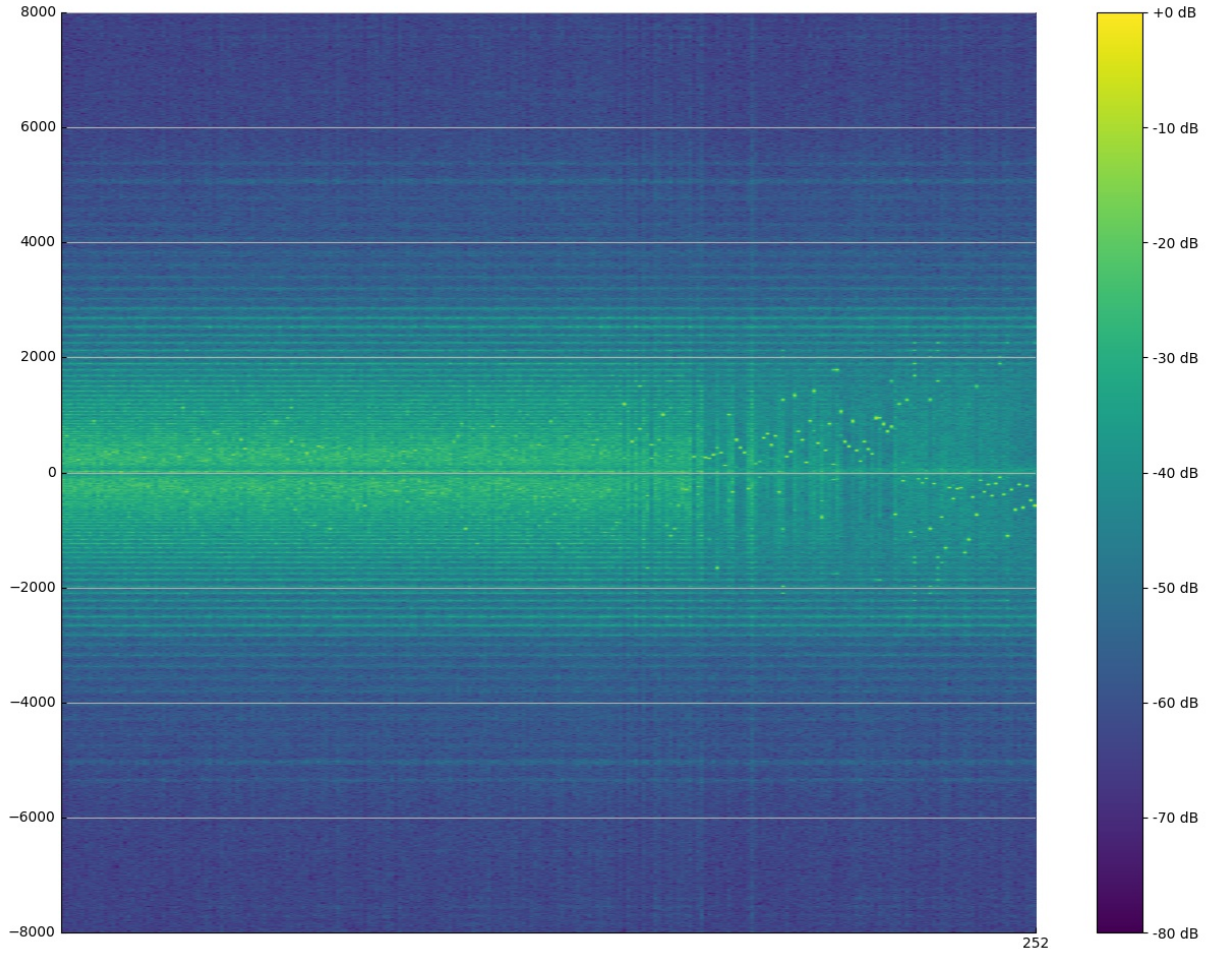


**Figure 8.** Frequency response of the entire filterbank for the *cl+rnd* experiment, ordered by spectral centroid.

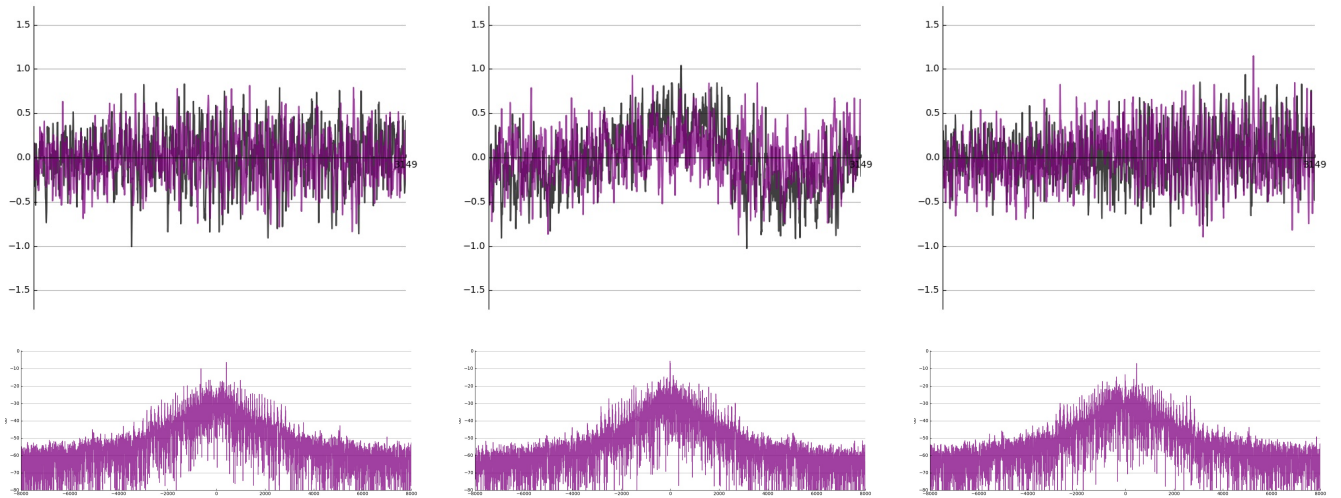


**Figure 9.** Examples of noisy filters from the *cl+rnd* experiment.



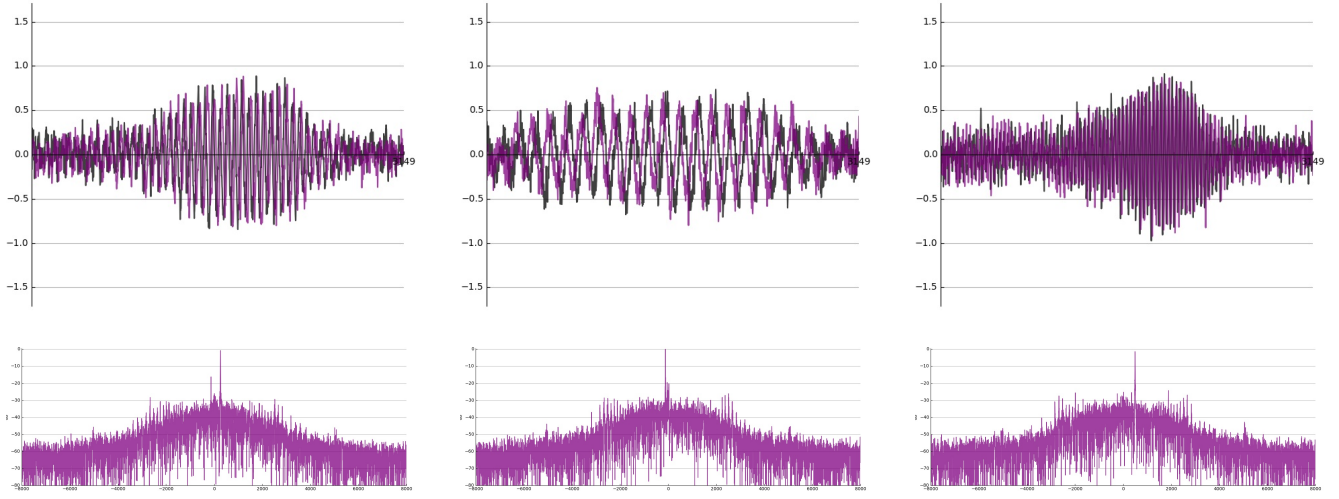


**Figure 10.** Examples of filters with a single prominent fundamental frequency from the *cl+rnd* experiment.

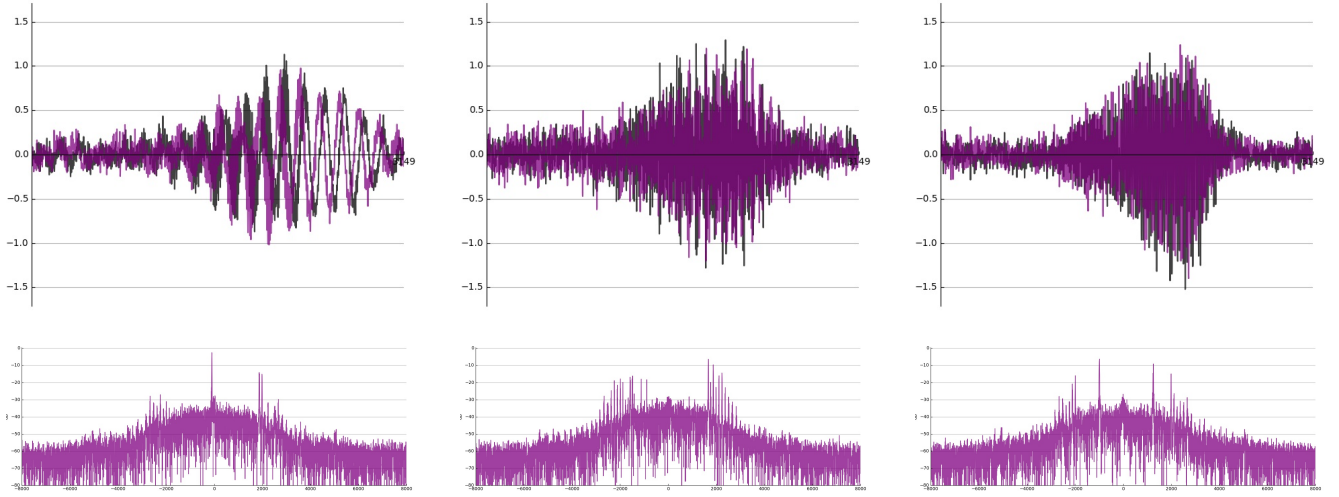


**Figure 11.** Examples of filters with multiple prominent fundamental frequencies from the *cl+rnd* experiment.

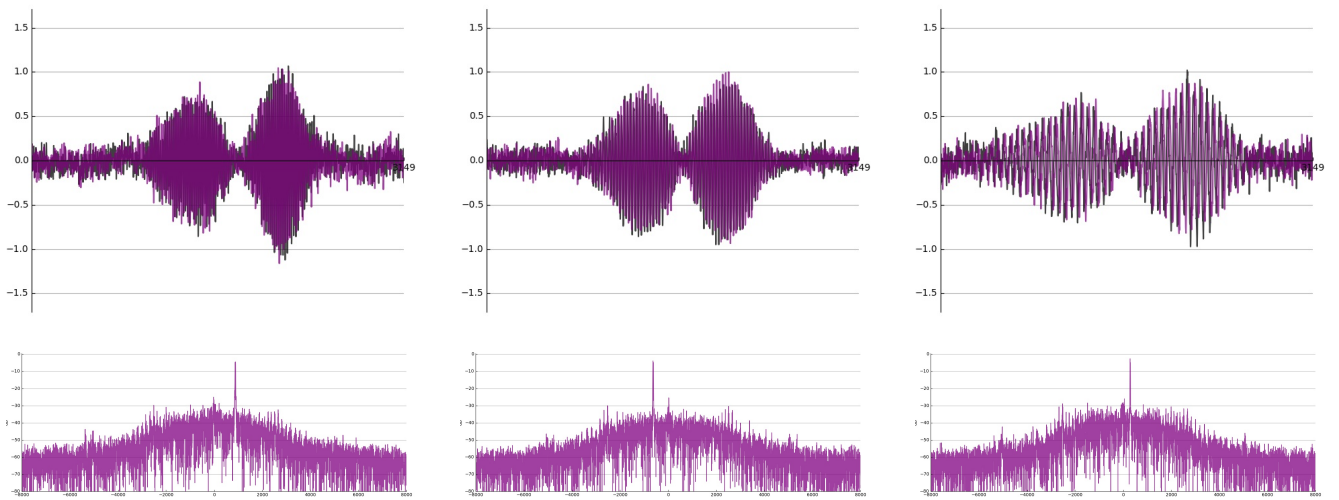


**Figure 12.** Examples of filters with two main lobes from the *cl+rnd* experiment.

### 9.3 Classic + VQT (cl+vqt)

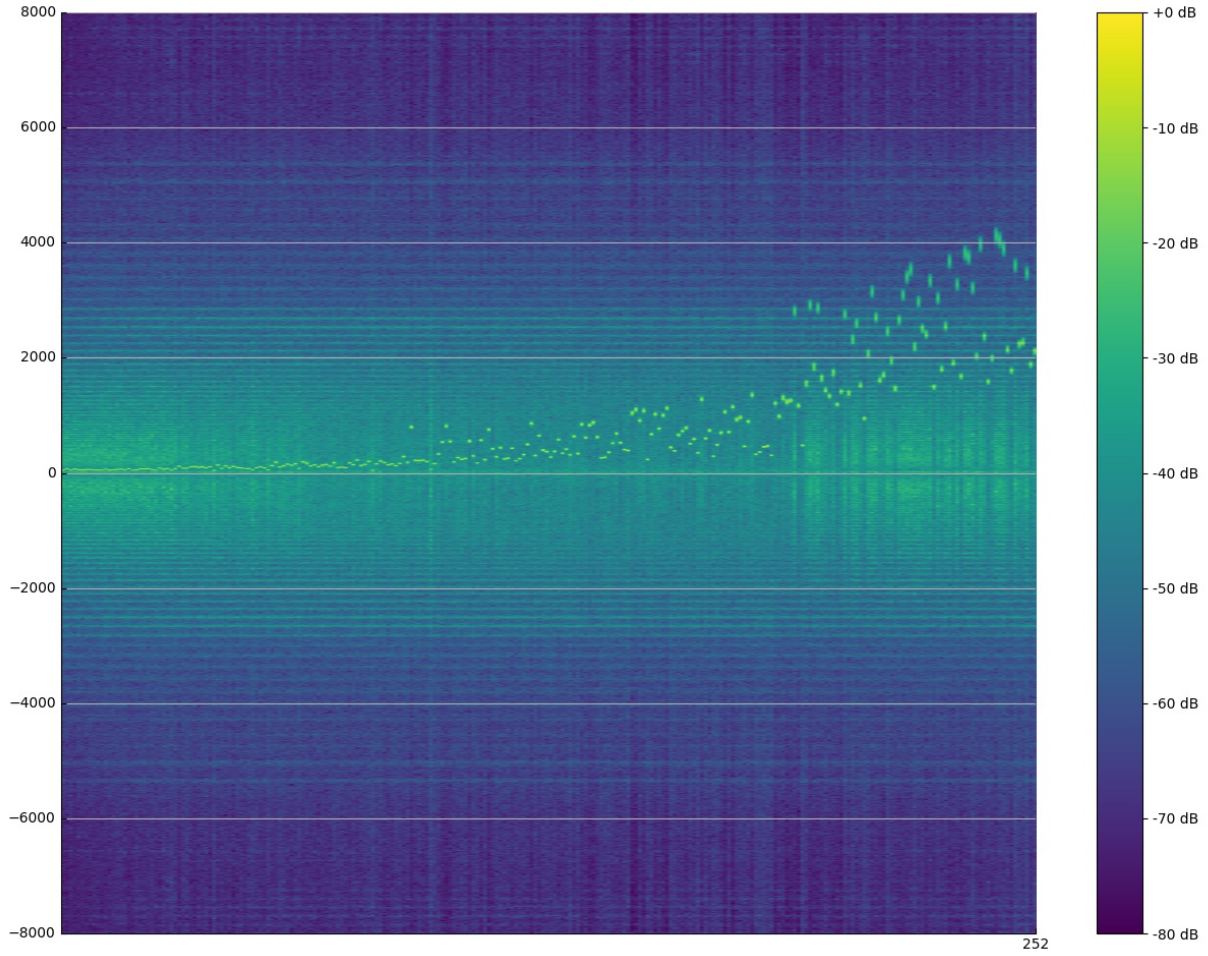


**Figure 13.** Frequency response of the entire filterbank for the *cl+vqt* experiment, ordered by spectral centroid.

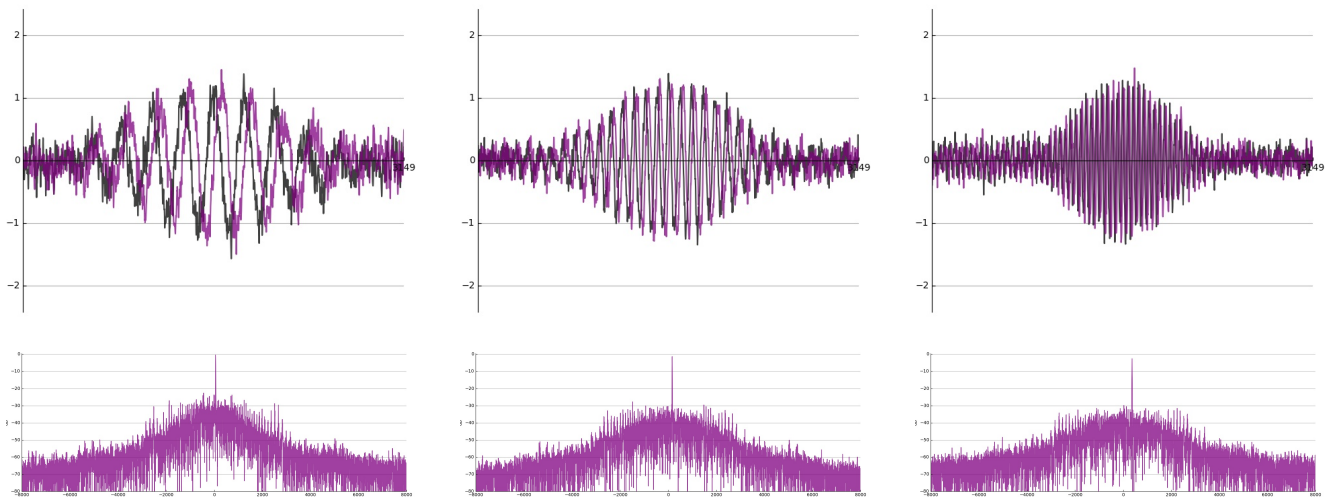


**Figure 14.** Examples of filters from the *cl+vqt* experiment which remain mostly intact with respect to the initialization.

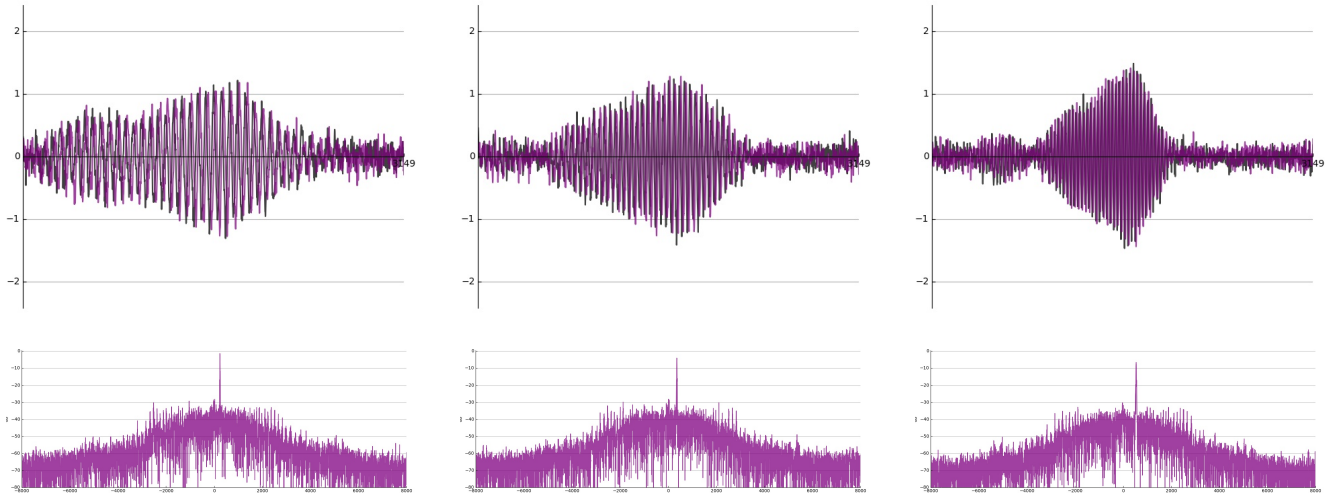


**Figure 15.** Examples of filters from the  $cl+vqt$  experiment with stretched impulse responses.

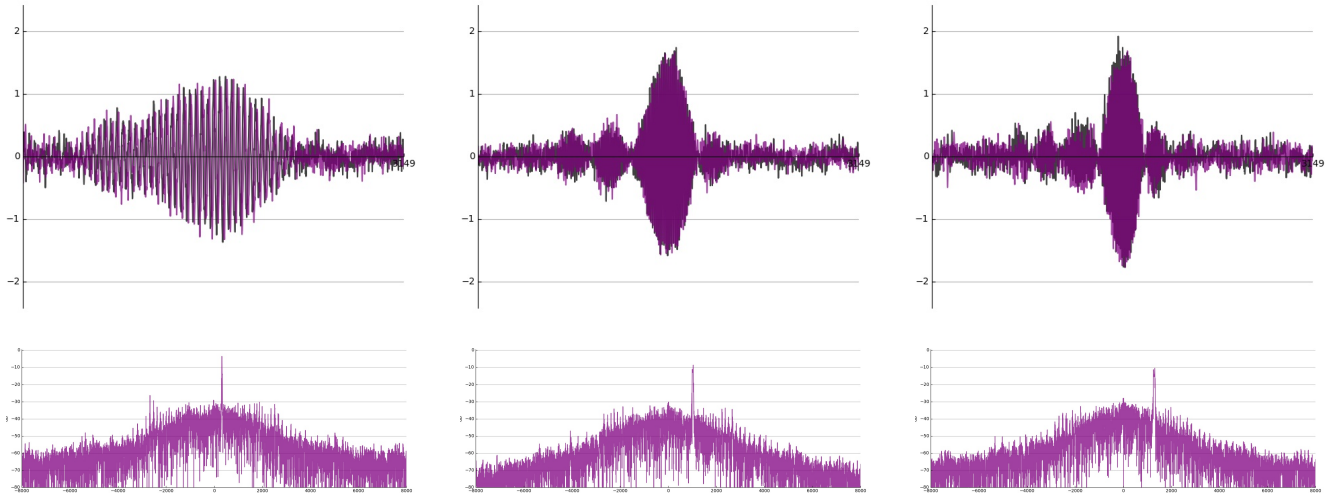


**Figure 16.** Examples of filters from the  $cl+vqt$  experiment where side-lobes in the waveform were introduced.

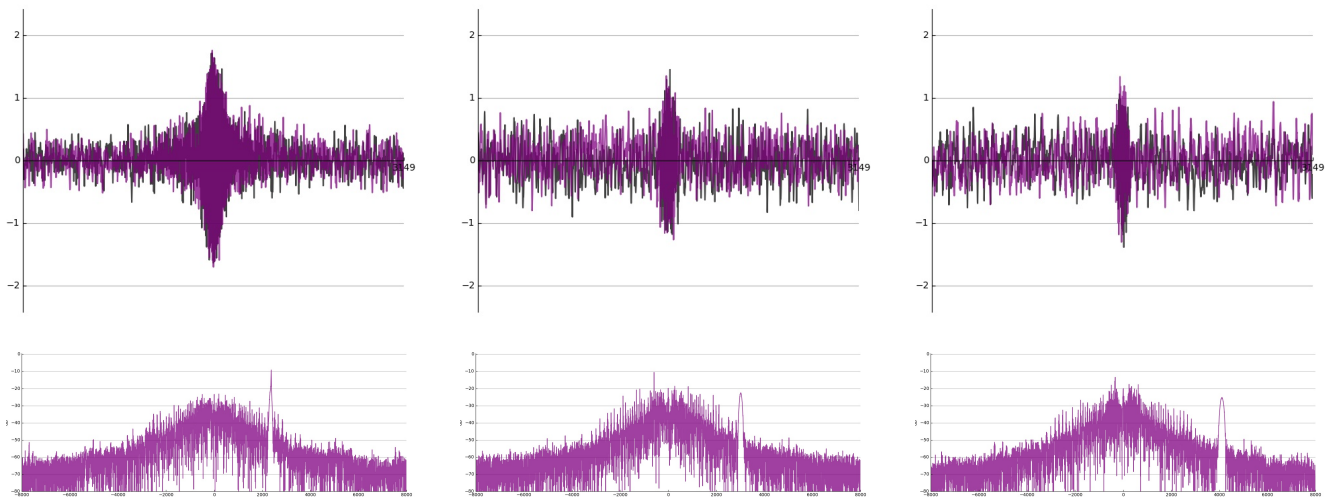


**Figure 17.** Examples of high-frequency filters from the  $cl+vqt$  experiment.



#### 9.4 Hilbert + Random (hb+rnd)

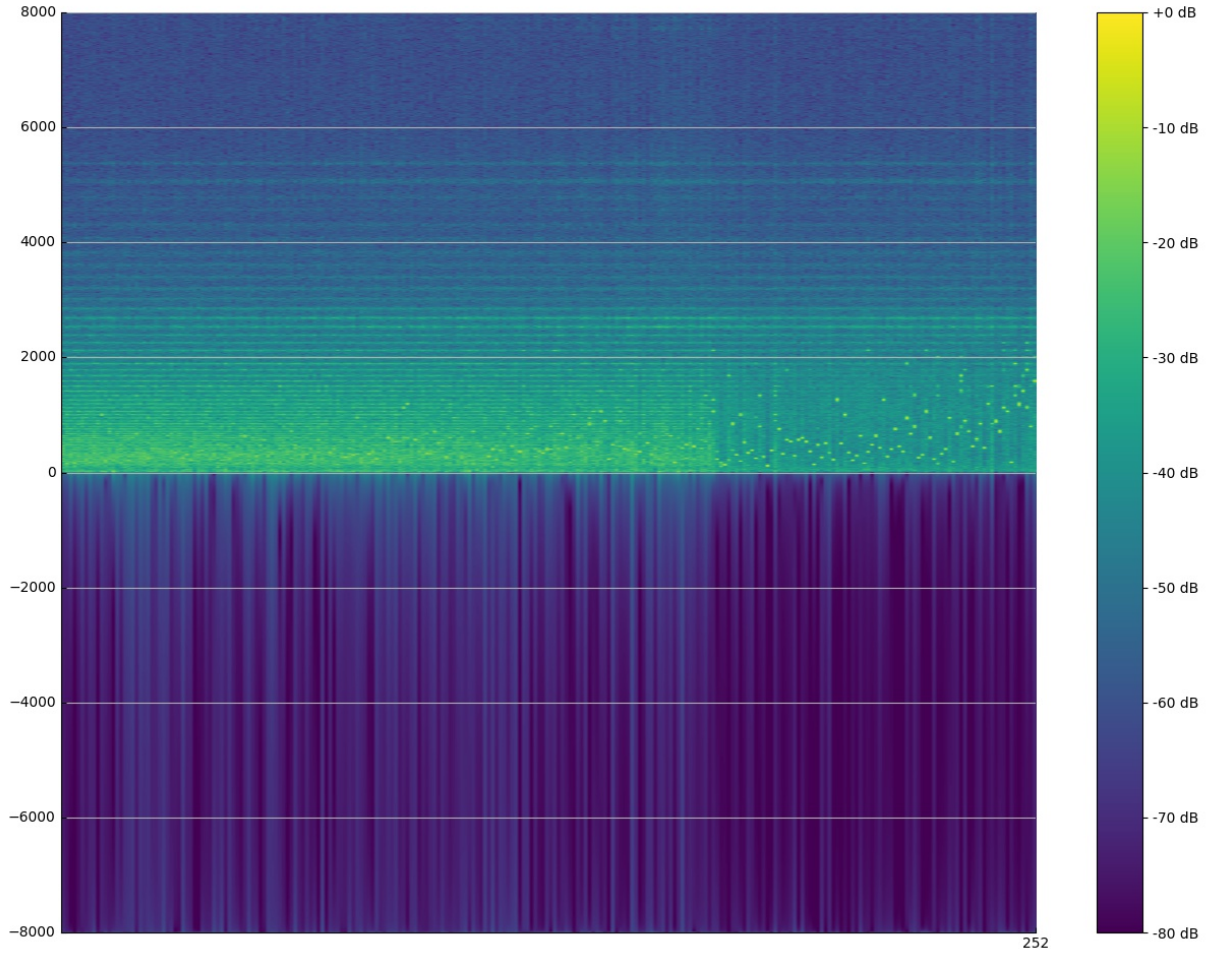


**Figure 18.** Frequency response of the entire filterbank for the *hb+rnd* experiment, ordered by spectral centroid.

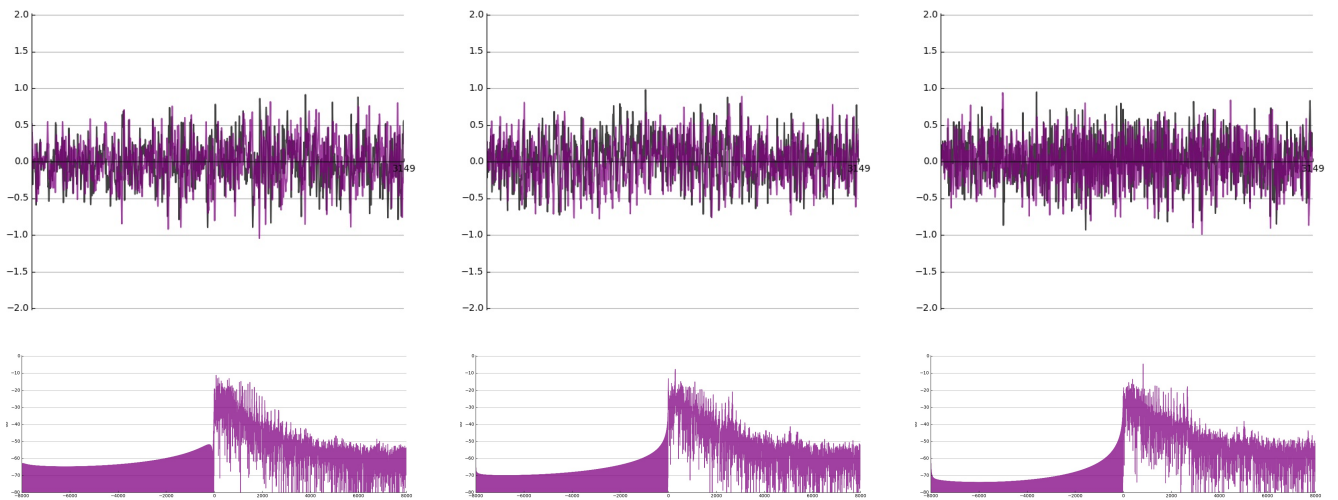


**Figure 19.** Examples of noisy filters from the *hb+rnd* experiment.

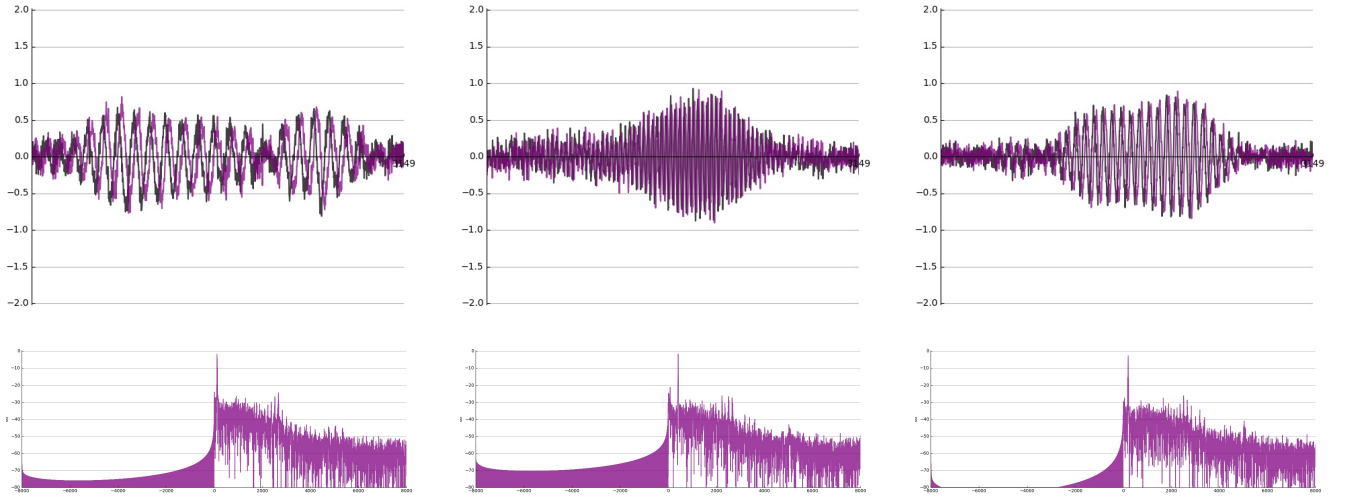


**Figure 20.** Examples of filters with a single prominent fundamental frequency from the *hb+rnd* experiment.

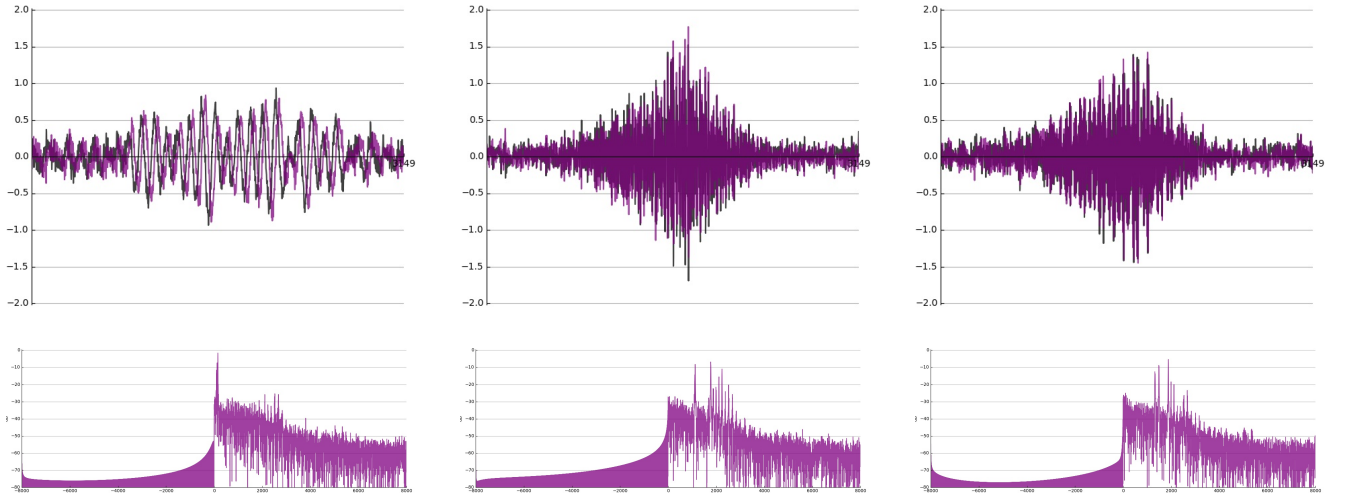


**Figure 21.** Examples of filters with multiple prominent fundamental frequencies from the *hb+rnd* experiment.

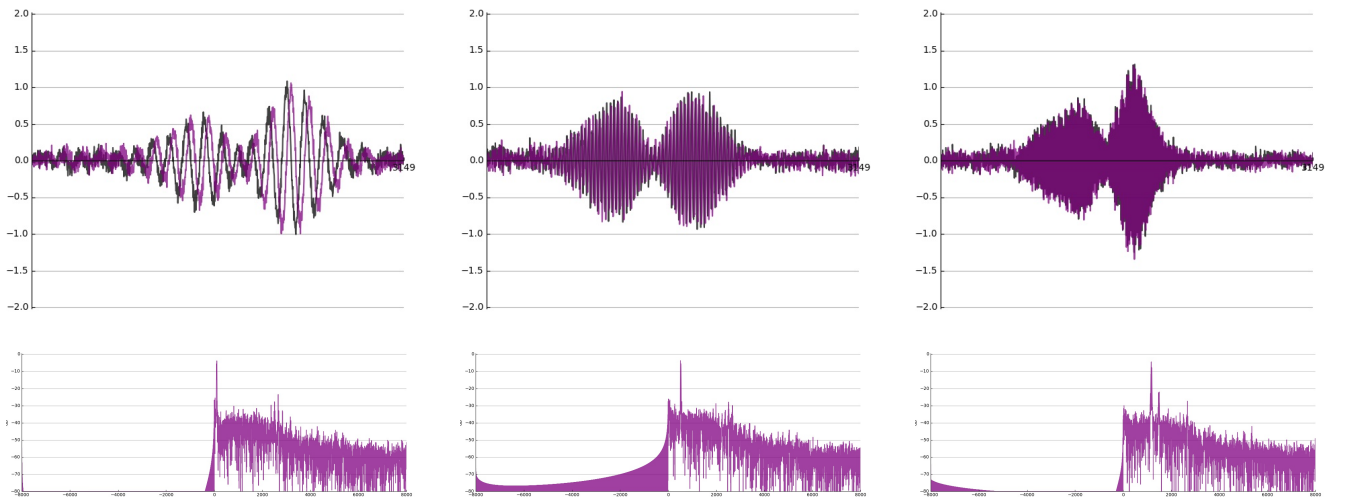


**Figure 22.** Examples of filters with two main lobes from the *hb+rnd* experiment.

## 9.5 Hilbert + VQT (hb+vqt)

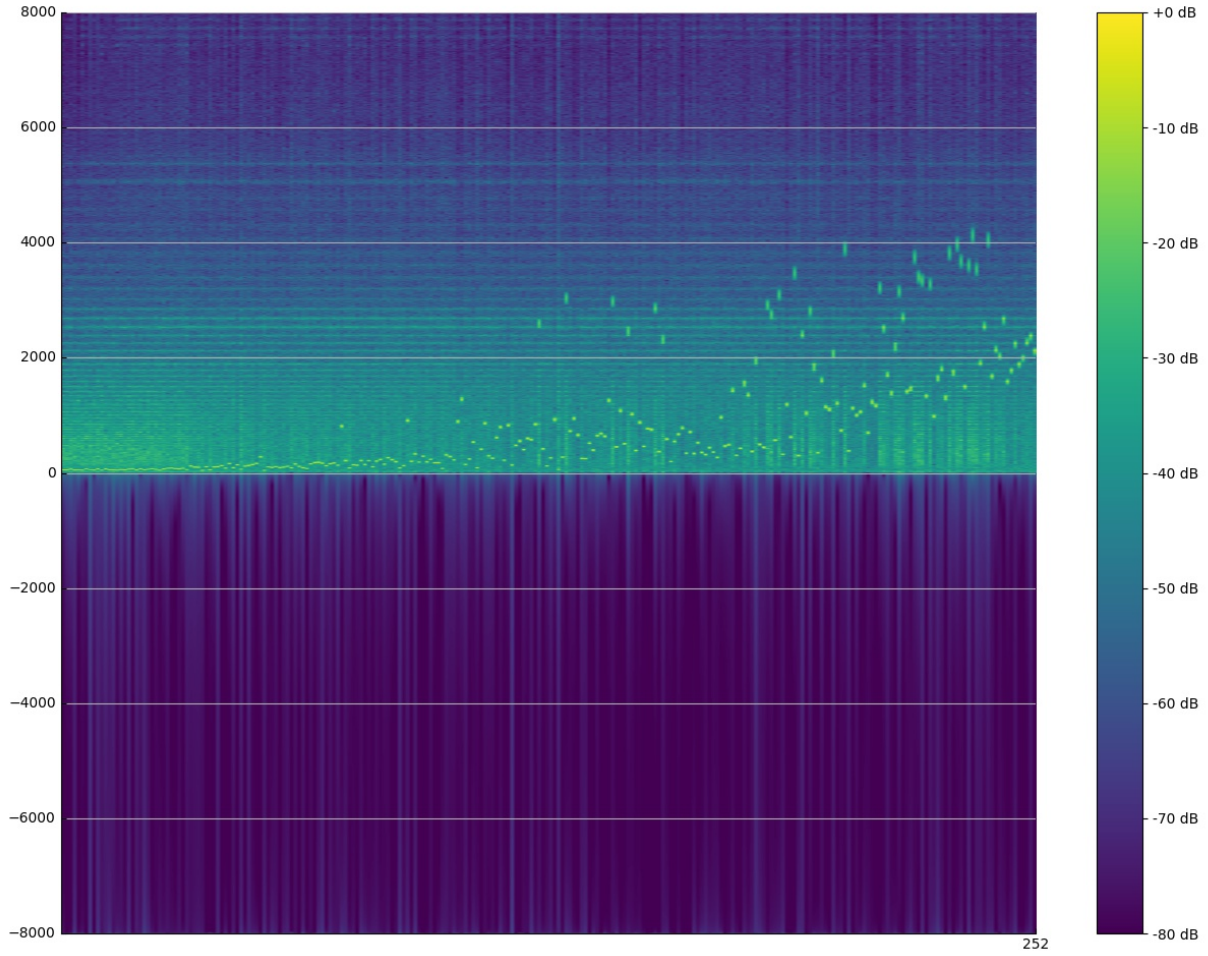


**Figure 23.** Frequency response of the entire filterbank for the *hb+vqt* experiment, ordered by spectral centroid.

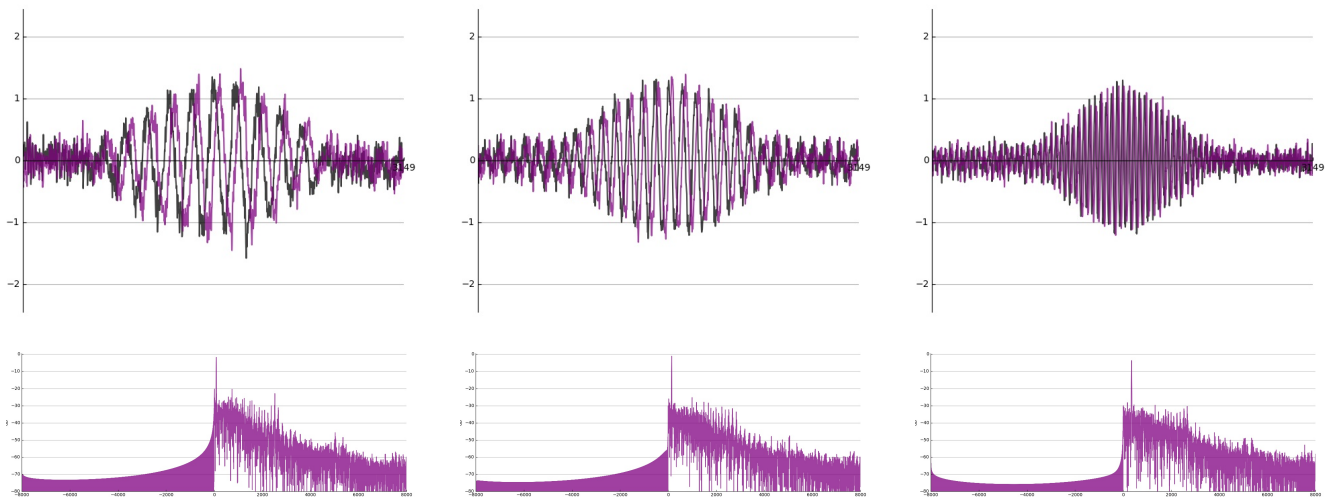


**Figure 24.** Examples of filters from the *hb+vqt* experiment which remain mostly intact with respect to the initialization.

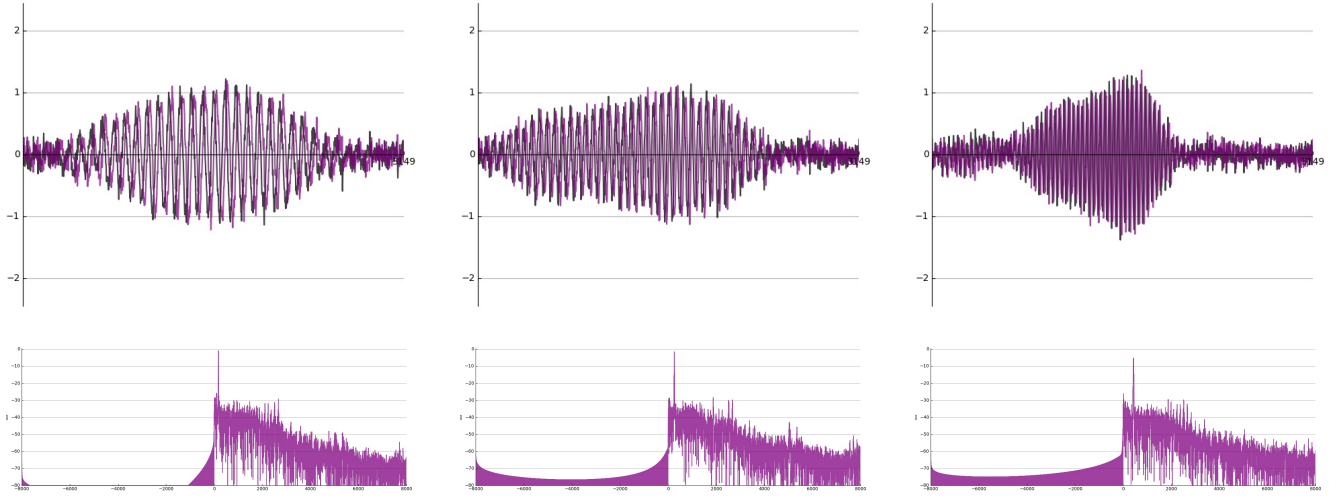


**Figure 25.** Examples of filters from the *hb+vqt* experiment with stretched impulse responses.

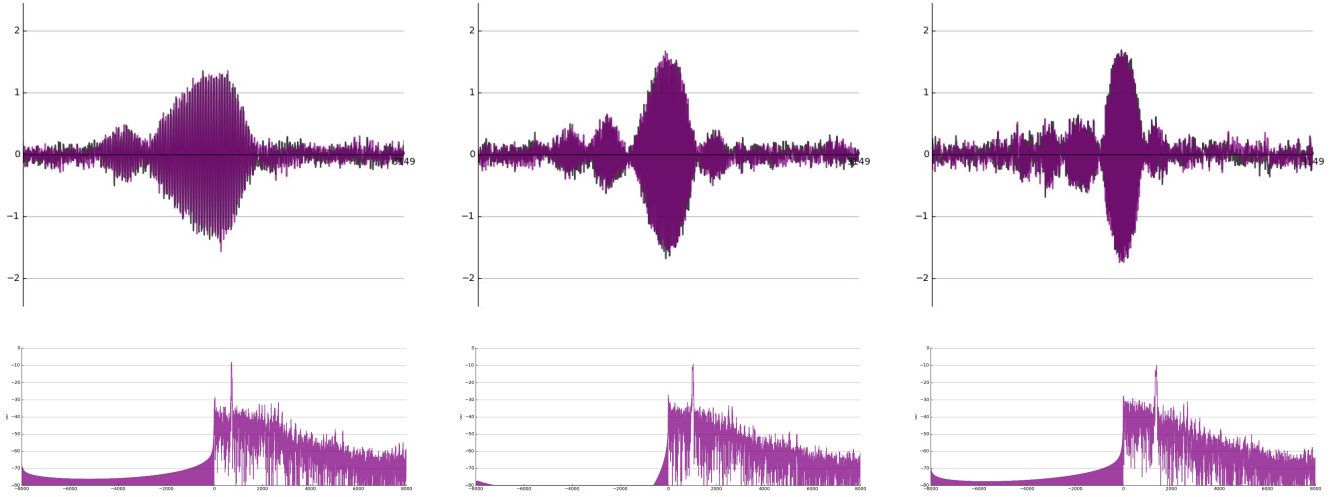


**Figure 26.** Examples of filters from the *hb+vqt* experiment where side-lobes were introduced.

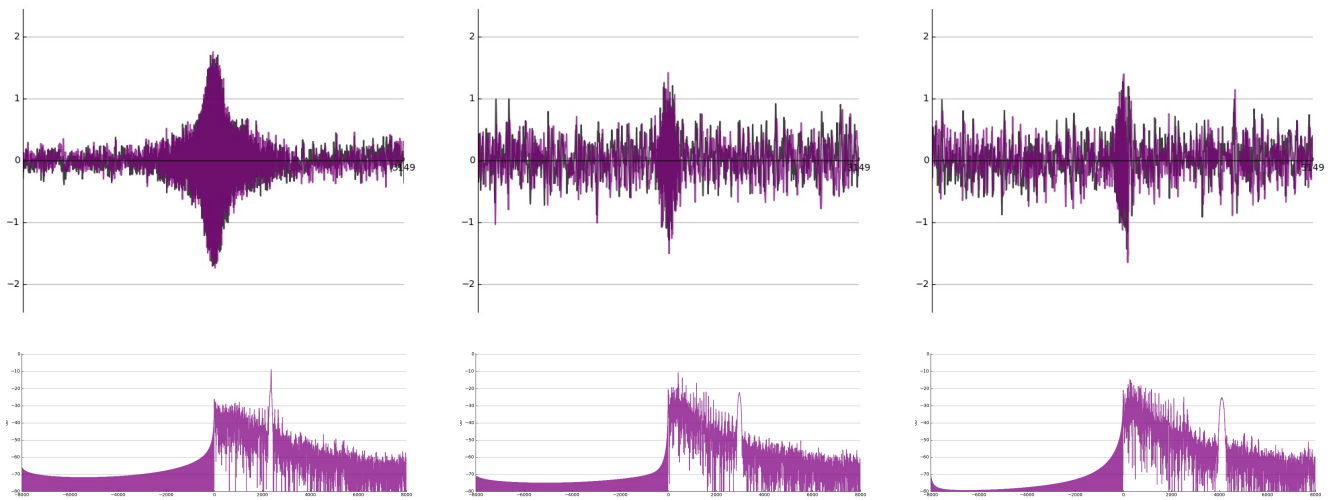


**Figure 27.** Examples of high-frequency filters from the *hb+vqt* experiment.



## 9.6 Hilbert + Random + Bernoulli (hb+rnd+brn)

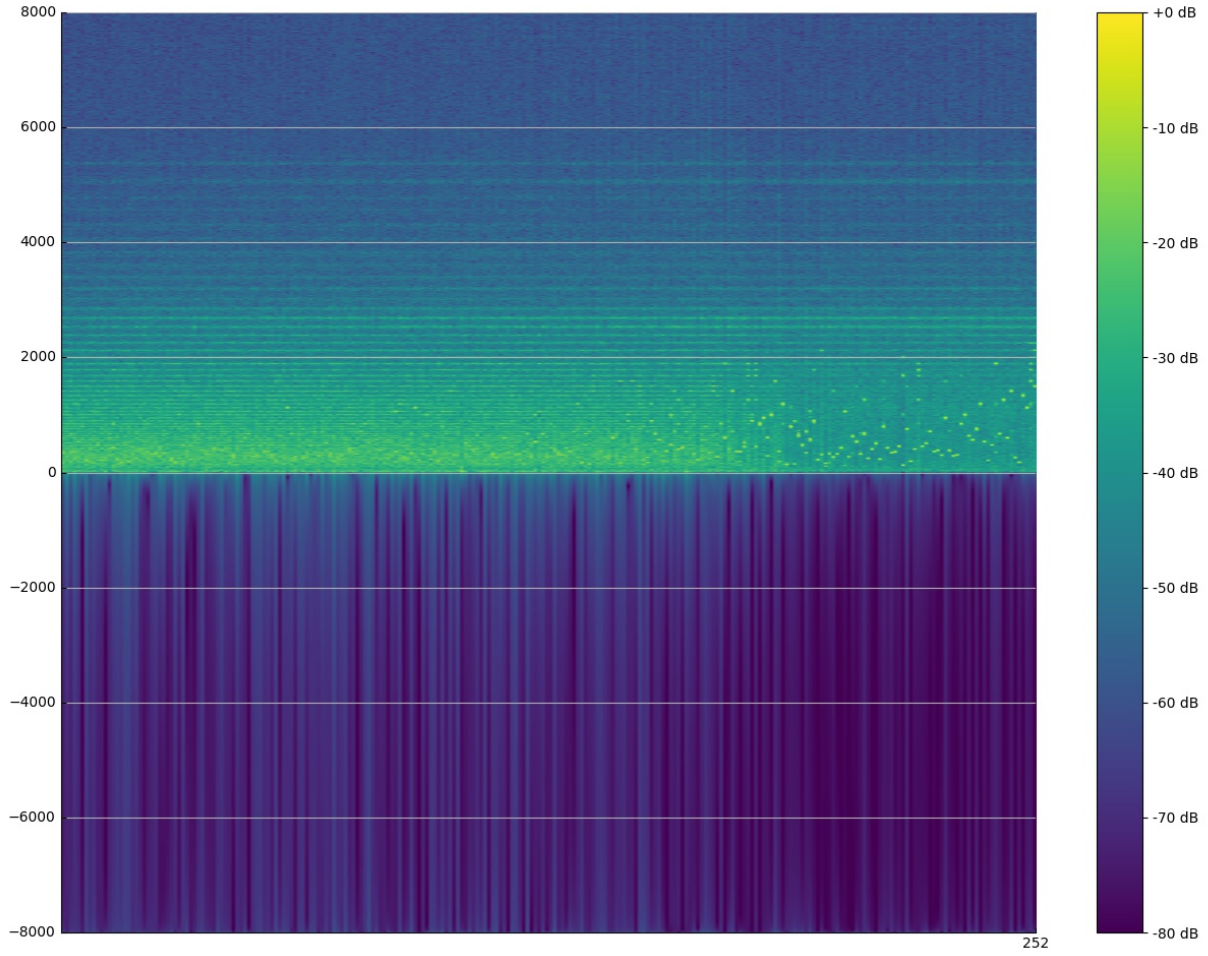


**Figure 28.** Frequency response of the entire filterbank for the *hb+rnd+brn* experiment, ordered by spectral centroid.

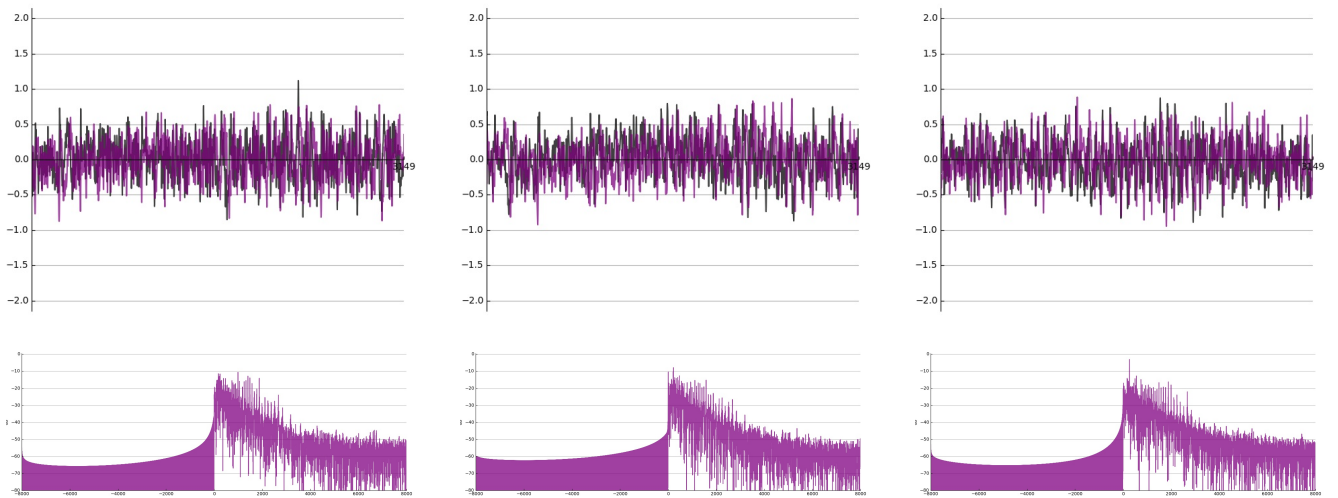


**Figure 29.** Examples of noisy filters from the *hb+rnd+brn* experiment.

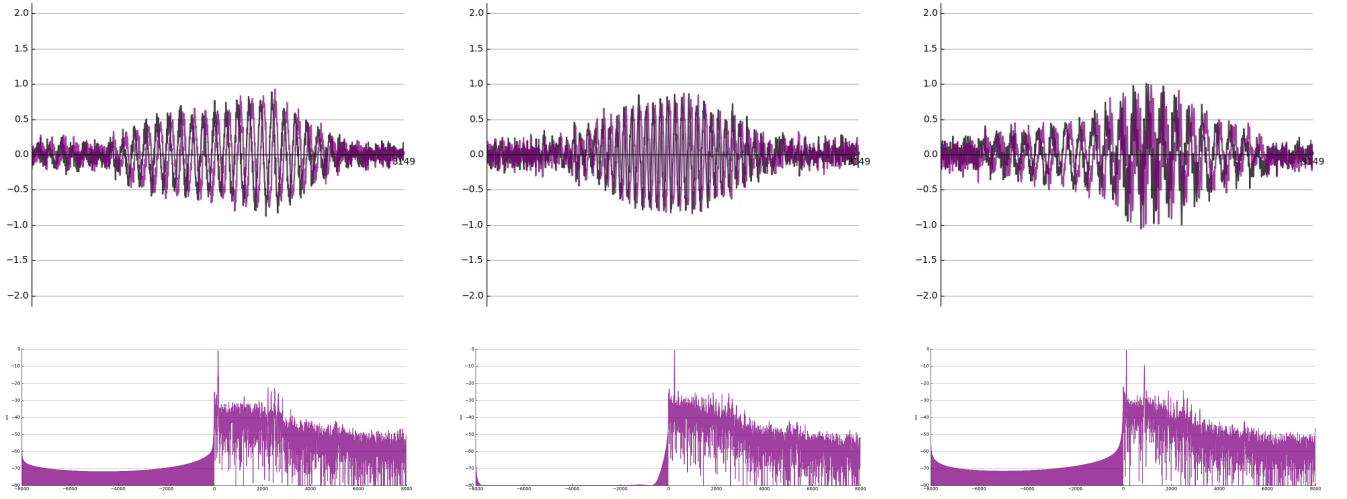


**Figure 30.** Examples of filters with a single prominent fundamental frequency from the  $hb+rnd+brn$  experiment.

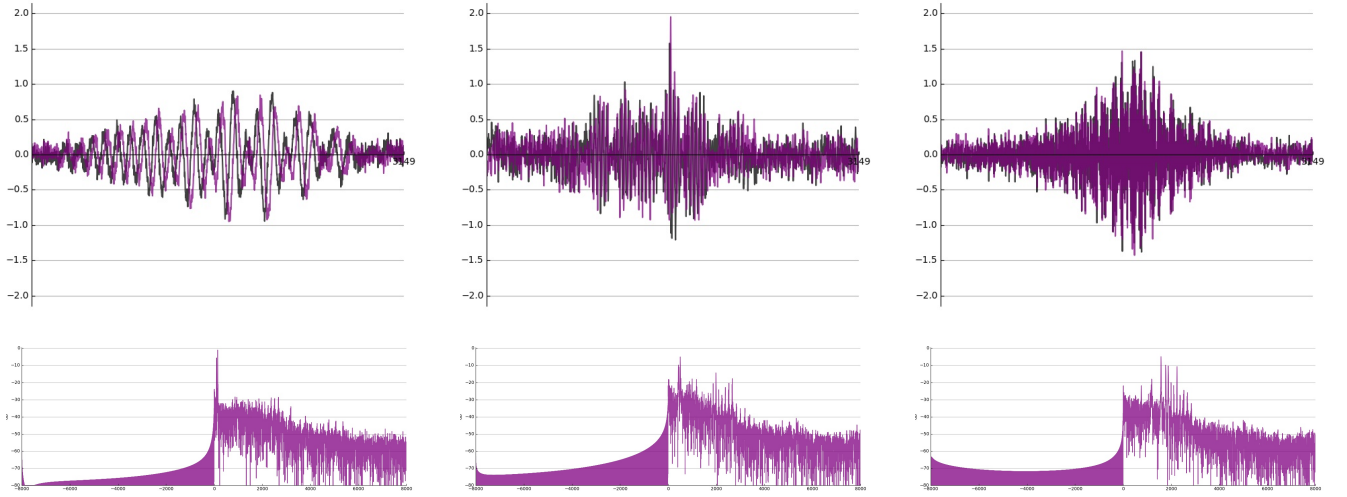


**Figure 31.** Examples of filters with multiple prominent fundamental frequencies from the  $hb+rnd+brn$  experiment.

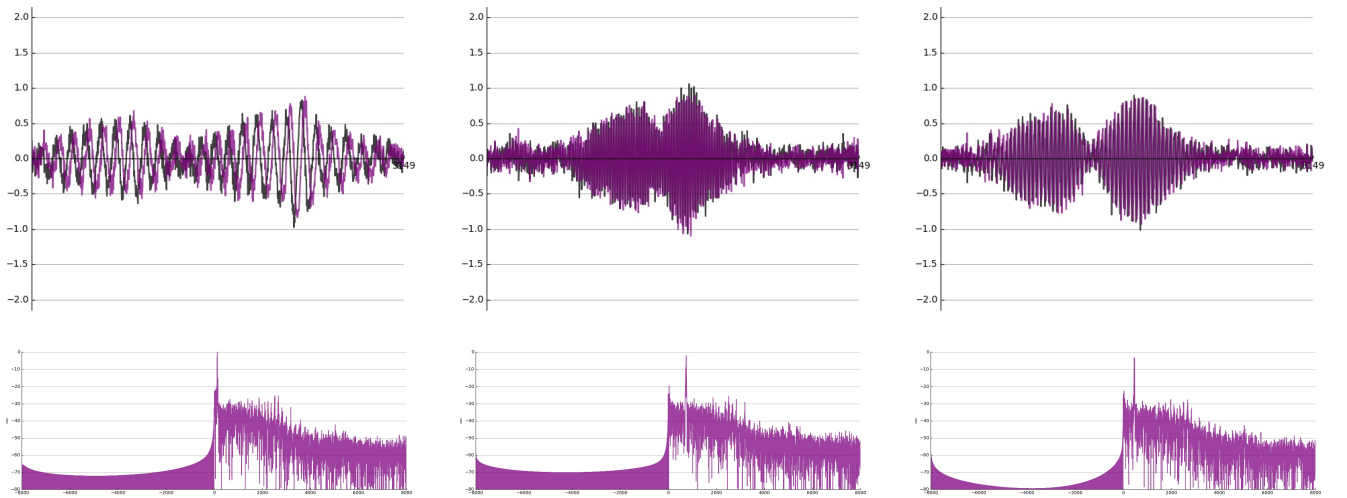


**Figure 32.** Examples of filters with two main lobes from the  $hb+rnd+brn$  experiment.

## 9.7 Hilbert + Random + Gaussian (hb+rnd+gau)

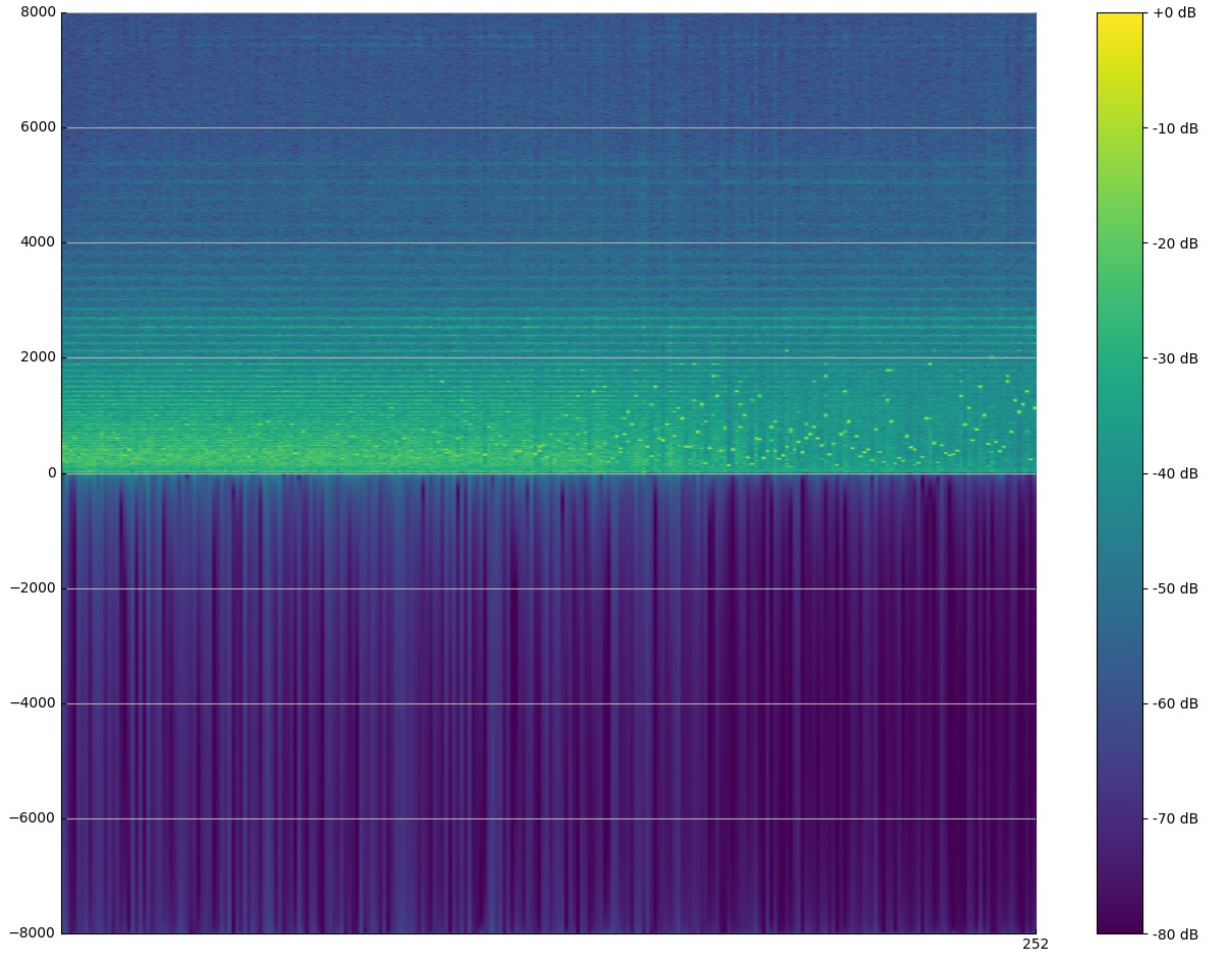


**Figure 33.** Frequency response of the entire filterbank for the *hb+rnd+gau* experiment, ordered by spectral centroid.

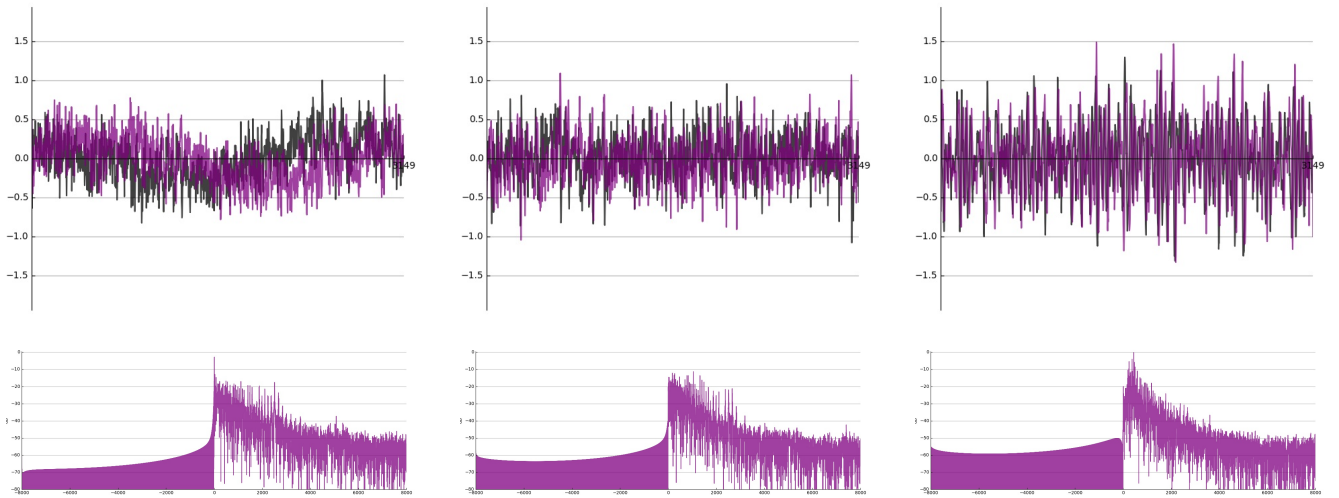


**Figure 34.** Examples of noisy filters from the *hb+rnd+gau* experiment.

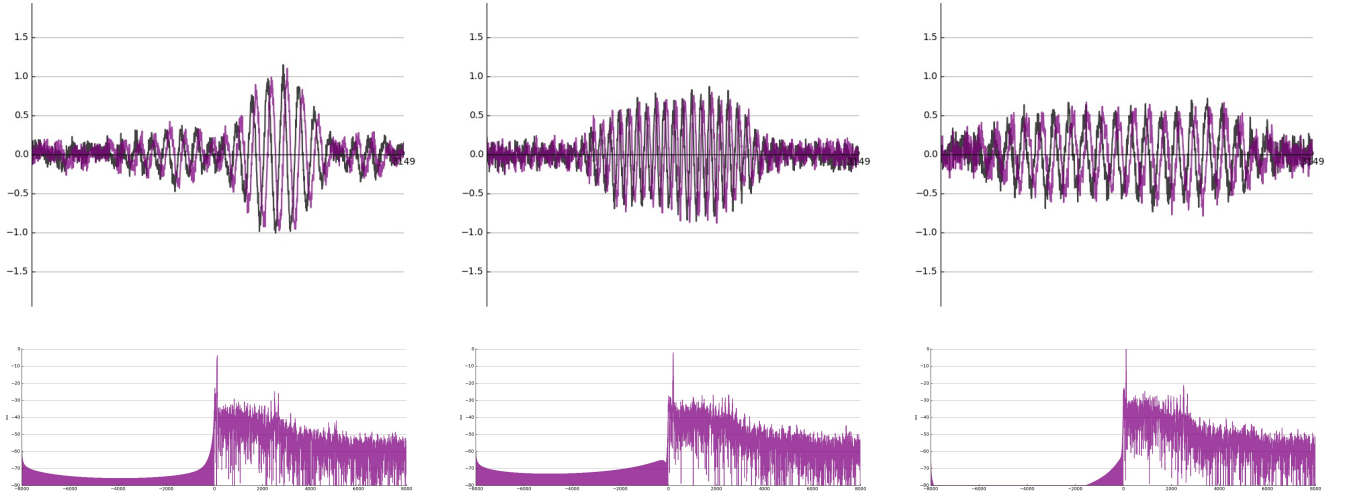


**Figure 35.** Examples of filters with a single prominent fundamental frequency from the *hb+rnd+gau* experiment.

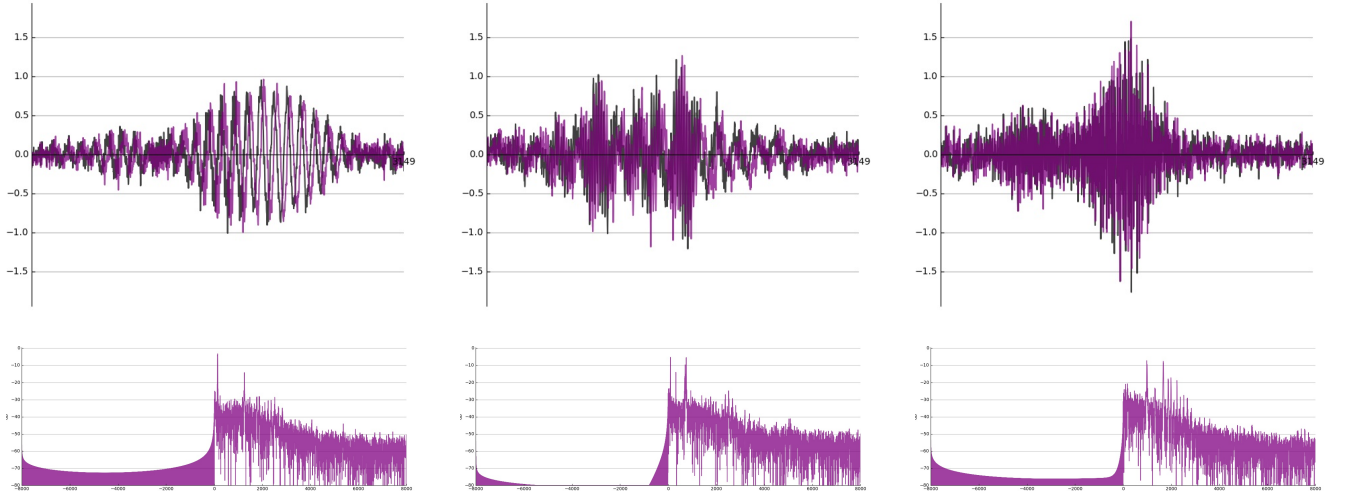


**Figure 36.** Examples of filters with multiple prominent fundamental frequencies from the *hb+rnd+gau* experiment.

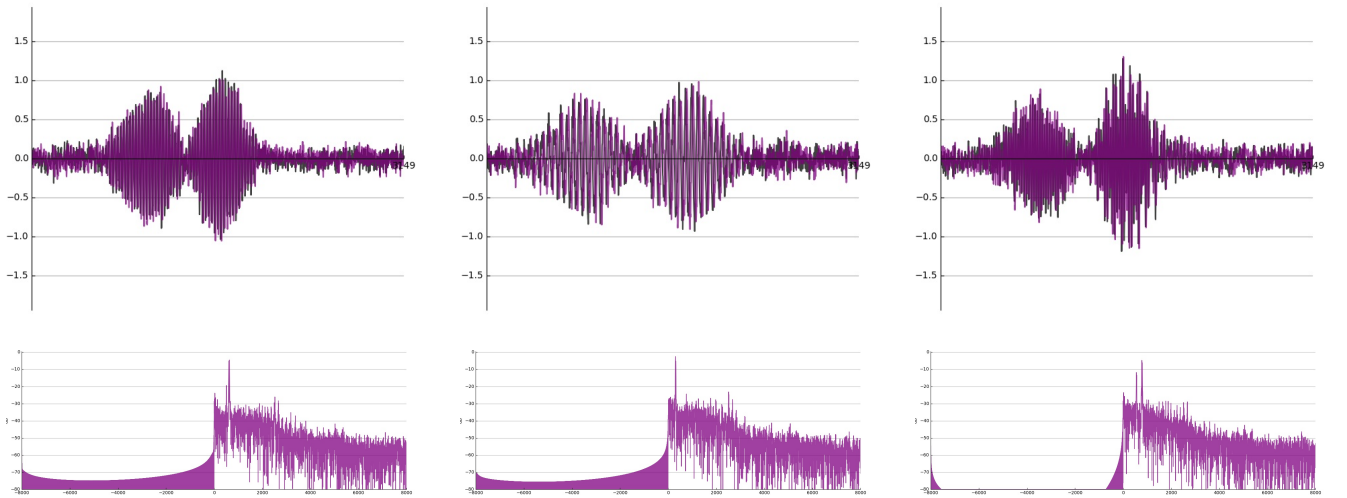


**Figure 37.** Examples of filters with two main lobes from the *hb+rnd+gau* experiment.



## 9.8 Hilbert + VQT + Variational (hb+vqt+var)

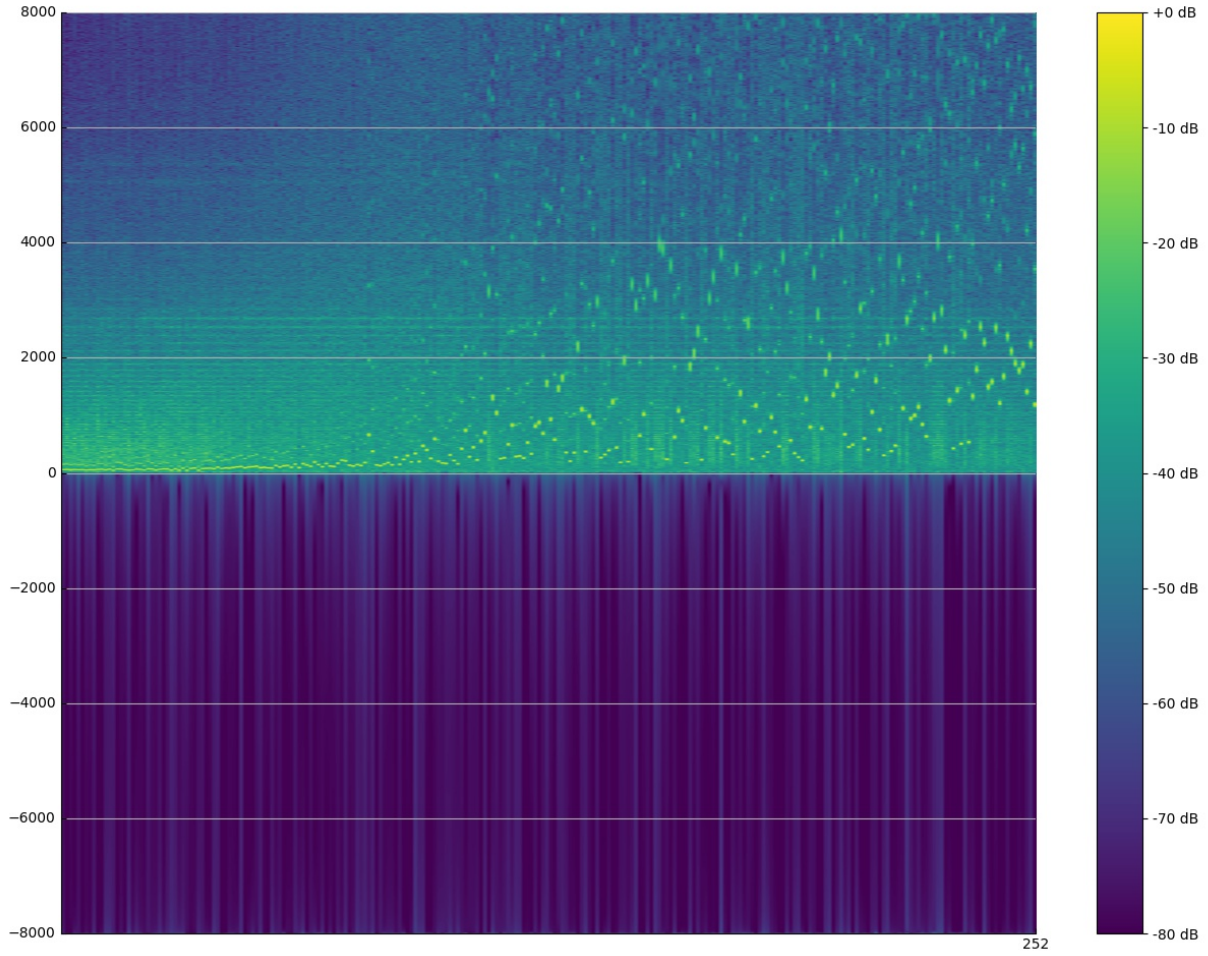


**Figure 38.** Frequency response of the entire filterbank for the *hb+vqt+var* experiment, ordered by spectral centroid.

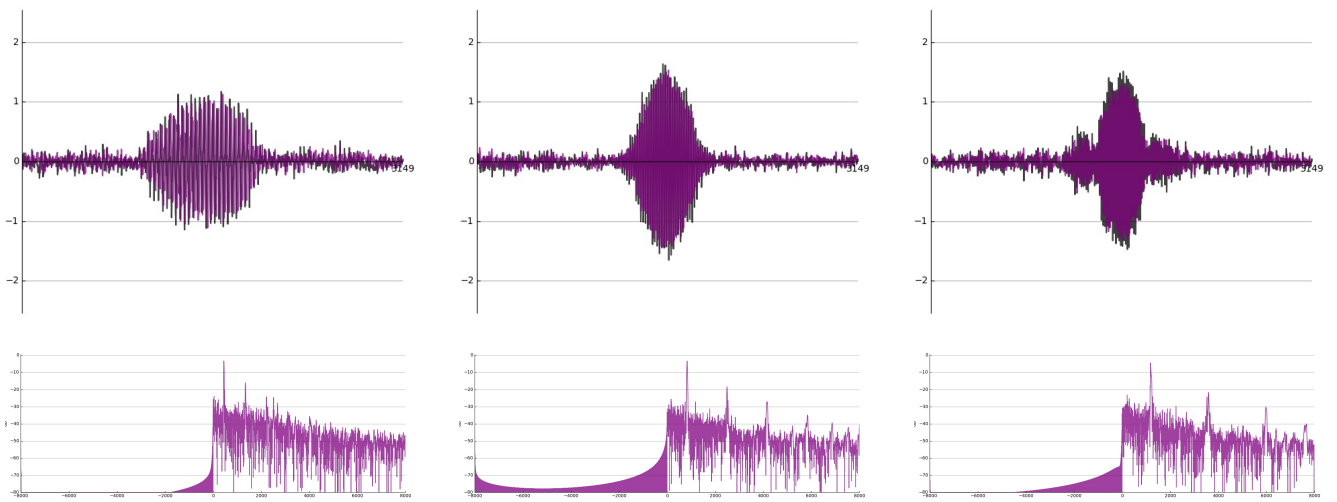


**Figure 39.** Examples of filters from the *hb+vqt+var* experiment where harmonics were introduced.

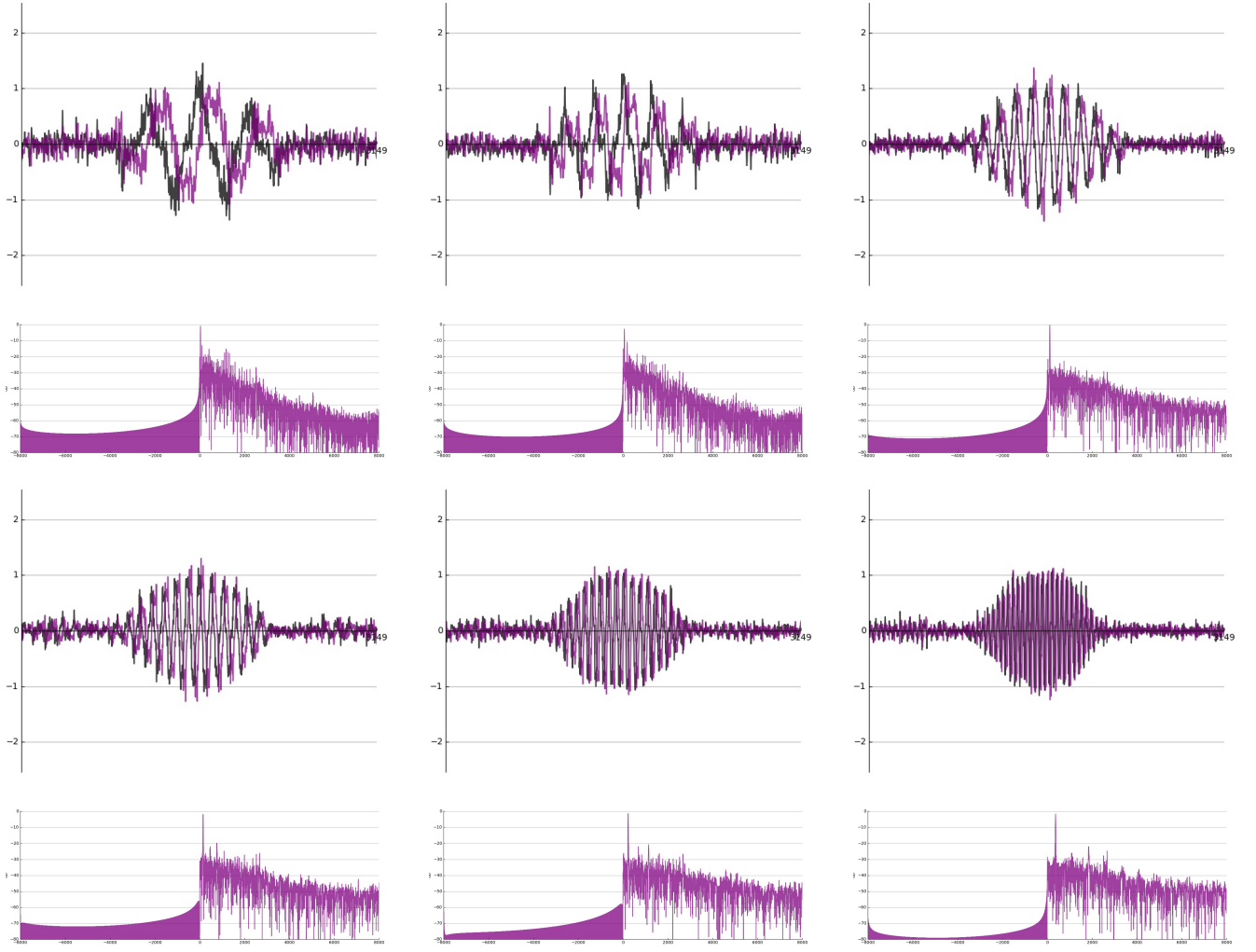


**Figure 40.** Examples of sparsified filters from the  $hb+vqt+var$  experiment.

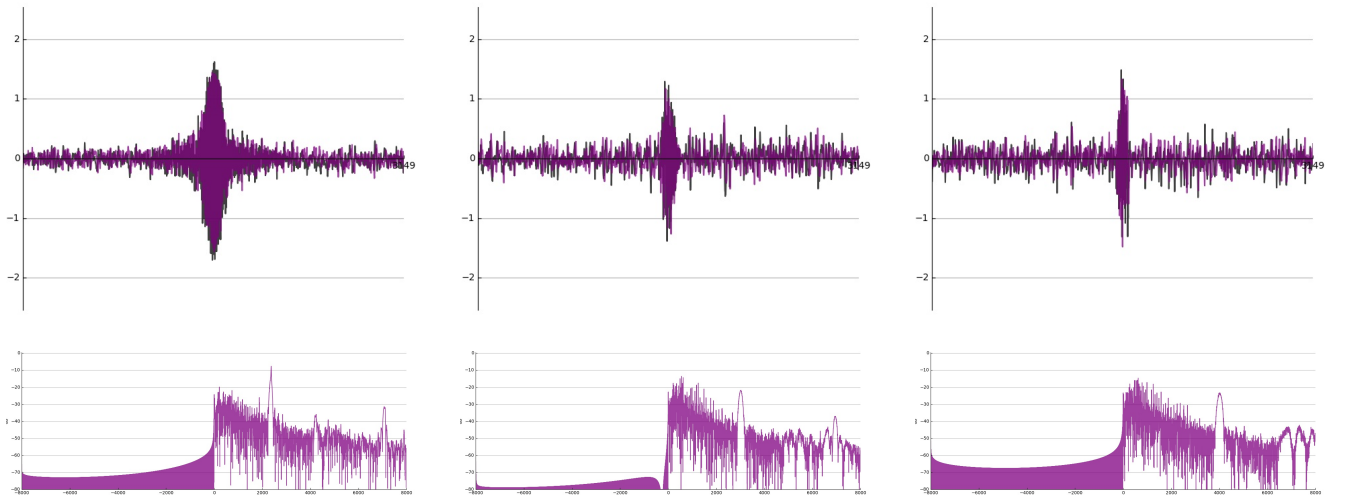


**Figure 41.** Examples of high-frequency filters from the  $hb+vqt+var$  experiment.

## 9.9 Hilbert + Comb + Variational (hb+comb+var)

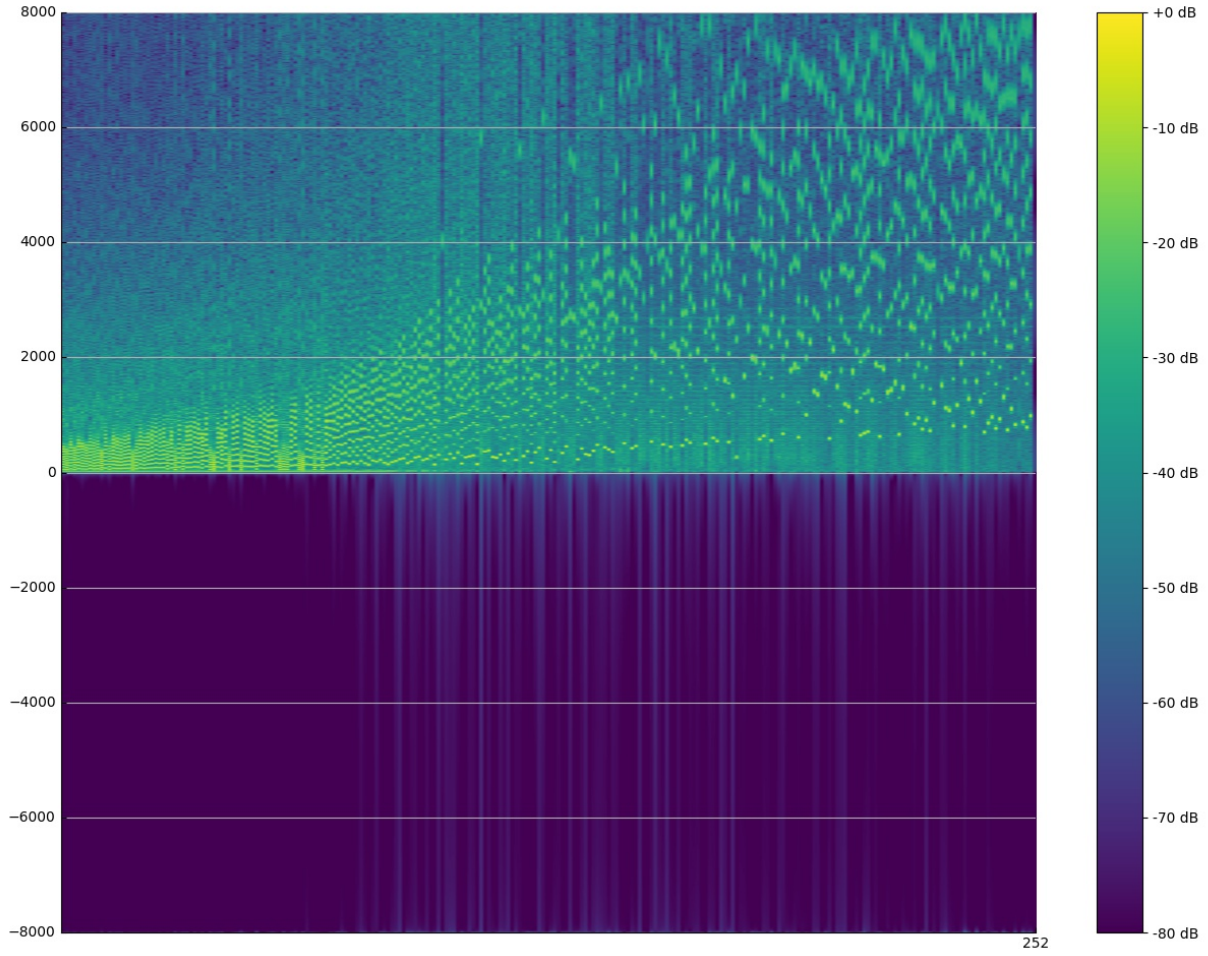


**Figure 42.** Frequency response of the entire filterbank for the *hb+comb+var* experiment, ordered by spectral centroid.

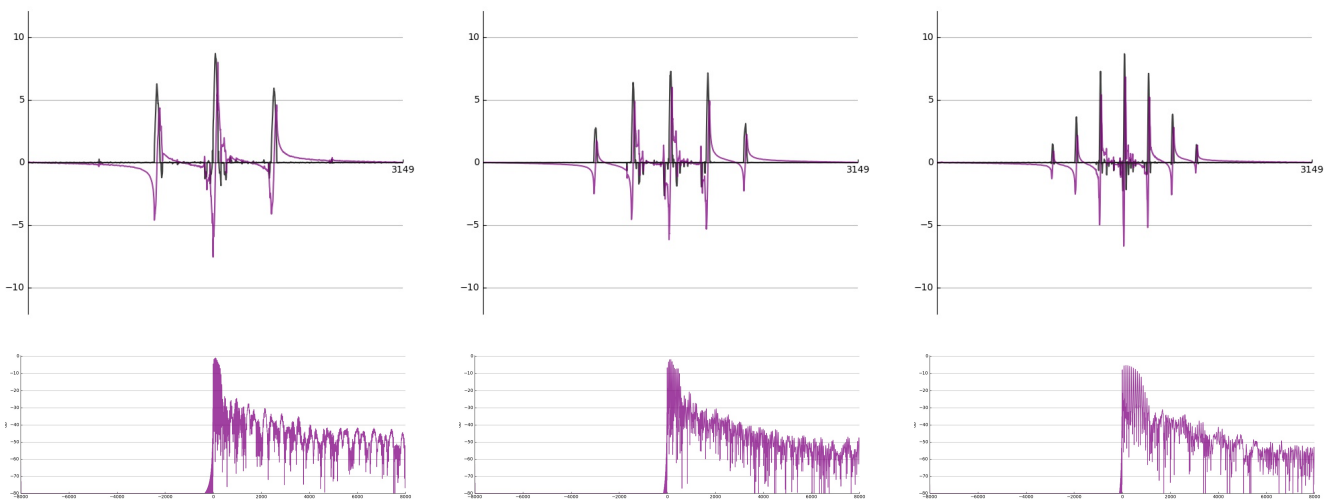


**Figure 43.** Examples of low-frequency filters from the *hb+comb+var* experiment.



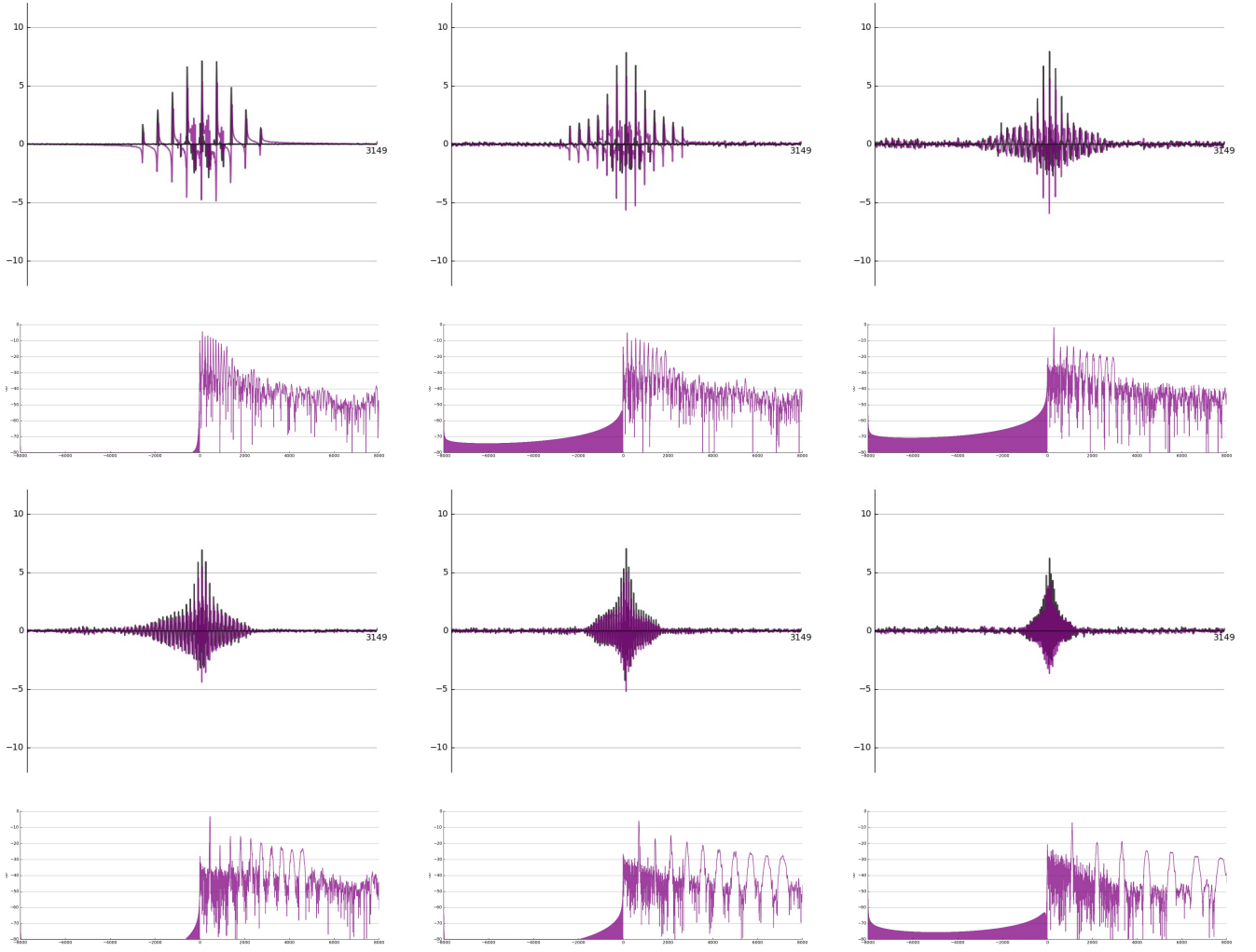


**Figure 44.** Examples of medium-frequency filters from the *hb+comb+var* experiment.

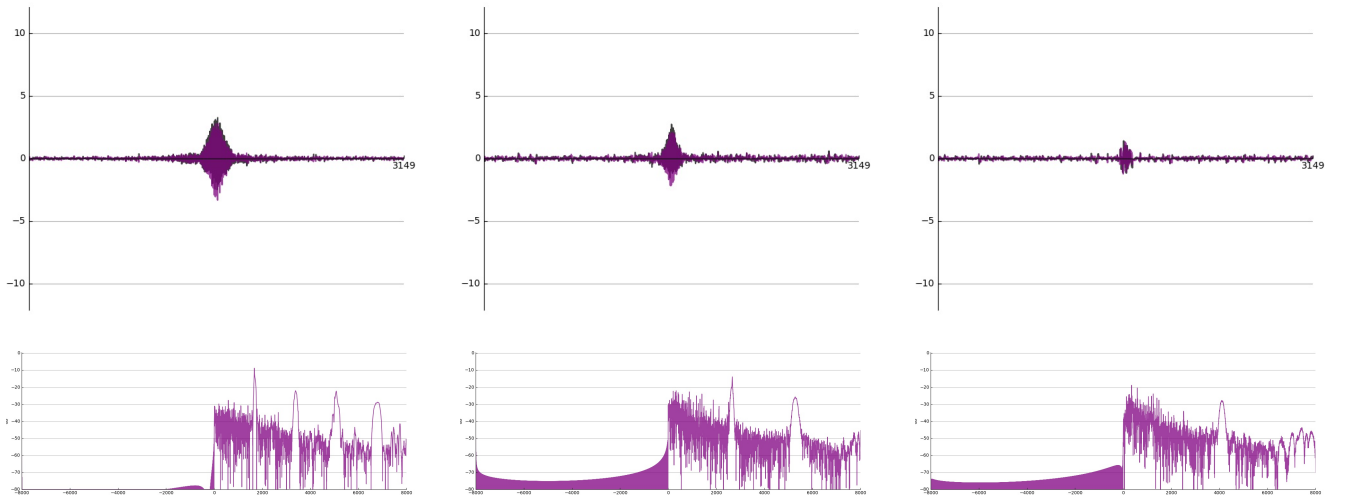


**Figure 45.** Examples of high-frequency filters from the *hb+comb+var* experiment.